Paleoceanography and Paleoclimatology

RESEARCH ARTICLE
10.1029/2021PA004371

# Coral-Based Sea Surface Salinity Reconstructions and the Role of Observational Uncertainties in Inferred Variability and Trends

**Emma V. Reed[1], Diane M. Thompson[1], and Kevin J. Anchukaitis[2,3]**

[1]Department of Geosciences, University of Arizona, Tucson, AZ, USA, [2]School of Geography, Development & Environment, University of Arizona, Tucson, AZ, USA, [3]Laboratory of Tree-Ring Research, University of Arizona, Tucson, AZ, USA

**Key Points:**

- A network of coral geochemical records reconstructs annual sea surface salinity across the global tropics (30°S–30°N) over the 20th century
- The leading modes of variability differ widely among salinity reanalyzes and objective analyses
- Reconstructed salinity shows hydrological variability associated with El Niño-Southern Oscillation, the Interdecadal Pacific Oscillation and Atlantic Multidecadal Oscillation, and long-term trends

**Supporting Information:**

Supporting Information may be found in the online version of this article.

**Correspondence to:**

E. V. Reed,
evreed@email.arizona.edu

**Citation:**

Reed, E. V., Thompson, D. M., & Anchukaitis, K. J. (2022). Coral-based sea surface salinity reconstructions and the role of observational uncertainties in inferred variability and trends. *Paleoceanography and Paleoclimatology*, *37*, e2021PA004371. https://doi.org/10.1029/2021PA004371

Received 16 OCT 2021
Accepted 20 MAY 2022



**Abstract** Climate observations in much of the tropical oceans are scarce during most of the 20th century, so paleoclimate proxies are needed to understand the full range of natural climate variability. Past proxy studies have focused primarily on sea surface temperatures, but there are comparatively few salinity reconstructions. Such reconstructions can extend our understanding of hydroclimate across the tropical oceans, including variability in precipitation, evaporation, and ocean circulation. Here we compile a network of salinity-sensitive coral $\delta^{18}O$ records, then apply a reduced-space method based on empirical orthogonal function analysis to reconstruct annual tropical salinity anomalies over the 20th century. A comparison of surface salinity data sets, including reanalyzes (SODA2/3, Ocean ReAnalysis System 5 (ORAS5), Global Ocean Data Assimilation System) and objective analyses (Institute of Atmospheric Physics (IAP), EN4, Delcroix), show large discrepancies in the spatial structure, temporal evolution, and importance of the leading modes of variability. Two salinity data sets, IAP and ORAS5, are retained for climate reconstruction. Our coral-based salinity reconstructions reveal significant long-term trends over the 20th century, which are likely associated with hydrological cycle intensification and possibly a weakening of the Walker Circulation. These reconstructions also capture the spatial and temporal patterns of salinity anomalies associated with the El Niño-Southern Oscillation, Interdecadal Pacific Oscillation, and Atlantic Multidecadal Oscillation. Ultimately, this approach can enhance our understanding of tropical hydroclimate prior to the observational era.

## 1. Introduction

Earth's tropical oceans influence major features of atmospheric circulation, including the Intertropical Convergence Zone (ITCZ), South Pacific Convergence Zone (SPCZ), and Walker and Hadley circulation, that affect global hydroclimate. These features display interannual and decadal variability that can drive widespread patterns of droughts and floods, and are likely undergoing long-term change as the global hydrological cycle intensifies with warming (Rhein et al., 2013). However, our understanding of long-term hydroclimate variability and trends over the global oceans is limited by sparse precipitation observations before the satellite era (1979–present) (Rhein et al., 2013; Schneider et al., 2017), with studies of 20th century precipitation generally relying on low-resolution (5°) precipitation products and reanalyzes (e.g., Green et al., 2017; Smith et al., 2012).

Paleoclimate reconstructions of sea surface salinity (SSS) can circumvent this limitation. SSS acts as a "rain gauge" that reflects the balance of precipitation with evaporation over the global oceans, and can also track regional changes in ocean circulation, terrestrial runoff and river discharge, and ice melt and formation, thus offering more comprehensive insight into hydroclimate than precipitation alone (Durack et al., 2012; Rhein et al., 2013; Skliris et al., 2014; Terray et al., 2012; N. T. Vinogradova & Ponte, 2013; Yu, 2011). In addition, salinity affects seawater density (and therefore ocean circulation and stratification), which has profound impacts on biological productivity and ocean heat storage (Rhein et al., 2013).

Despite its key role in circulation and climate variability, there is no "gold standard" (i.e., widely accepted as the most reliable) gridded salinity data set. SSS observations, like those of precipitation, are sparse across the tropical oceans for most of the 20th century (Figure 1) (Bingham et al., 2002). The two main approaches to infilling the sparse observational data come with their own challenges. The first approach, Objective Analysis (OA), filters and interpolates sparse salinity observations to generate a continuous gridded product. In the absence of observations, OA data sets typically relax to the SSS climatology in a given location (Table 1), masking variability and trends. In the second approach, ocean reanalyzes attempt to bridge this observational void, assimilating salinity

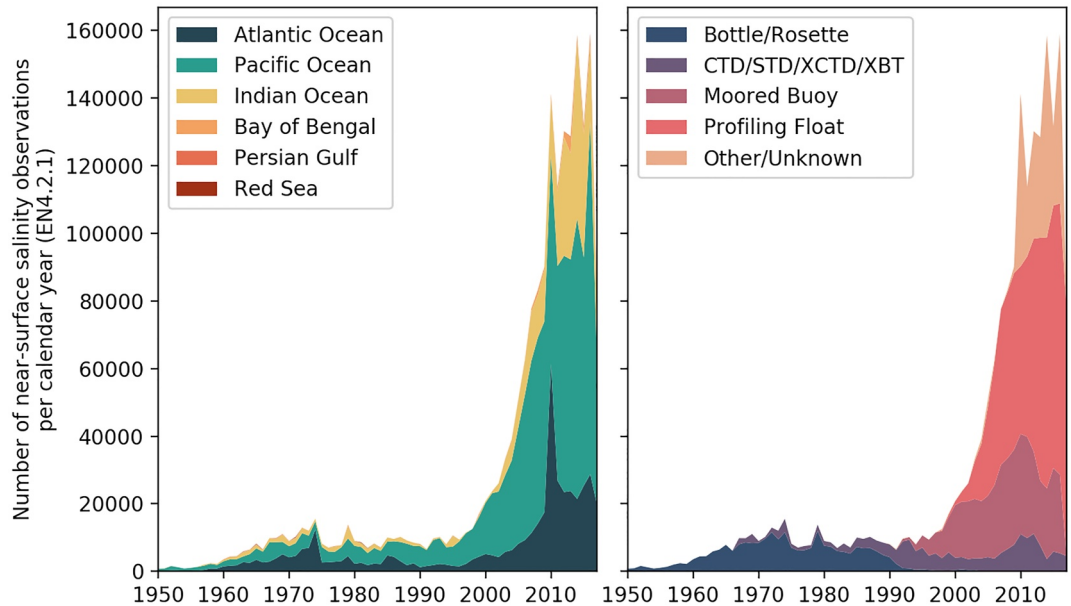


**Figure 1.** The number of observations per region (left) and instrumentation type (right) of near-surface (≤10 m) salinity observations in the global tropics (30°S–30°N, 1950–2017). Data are compiled from quality-controlled EN4.2.1 profiles (Good et al., 2013), which include observations from Argo (Argo, 2020), the Global Temperature and Salinity Profile Program (Sun et al., 2010), and the World Ocean Database (Boyer et al., 2013).

observations into a numerical model forced by other variables (e.g., ocean temperature, precipitation, and wind stress) (Storto et al., 2019). In this way, observations are used to "nudge" the model estimate of the salinity field toward the observational state at regular intervals (either online or offline). However, reanalyzes can still be sensitive to changes in the frequency, location, or method of observations and are strongly susceptible to model biases (Huang et al., 2008; Xue et al., 2017). Recent improvements in ocean reanalyzes, including higher resolution models, more realistic physics and atmospheric forcing, better quality control of observations, and improved data assimilation methods, broaden the potential applications of reanalysis data (Storto et al., 2019). These applications include the use of salinity reanalyzes for calibration of coral paleoclimate records in the absence of in situ observations.

Coral geochemical proxies have been widely applied to reconstruct tropical climate variability and trends, particularly of sea surface temperature (SST). Such reconstructions provide insights into natural climate variability, such as the El Niño-Southern Oscillation (ENSO), as well as anthropogenic trends, over longer time scales than the instrumental record. Coral-based SST reconstructions include regionally representative time series (e.g., Abram et al., 2003, 2008; Abram, Wright, et al., 2020; Cobb et al., 2003, 2013; Grothe et al., 2020; Hendy, 2002; Linsley et al., 2004, 2006, 2015; Tierney et al., 2015), paleo-data assimilation (Sanchez et al., 2021), and field reconstructions (Evans et al., 2000, 2002), including Regularized Expectation Maximization field reconstruction methods (Emile-Geay et al., 2013b; Sanchez et al., 2020). However, the most common coral geochemical proxy, $\delta^{18}O$, does not solely record an SST signal. Instead, coral $\delta^{18}O$ reflects a combination of both SST and seawater $\delta^{18}O$. In the tropical-subtropical oceans, seawater $\delta^{18}O$ depends on the balance of precipitation, evaporation, diffusion, advection, and runoff/river outflow, and therefore covaries with SSS at many coral sites (Cahyarini et al., 2008; Cole & Fairbanks, 1990; Conroy et al., 2017; Fairbanks et al., 1997; LeGrande & Schmidt, 2006; Thompson et al., 2011). The relative contribution of seawater $\delta^{18}O$ and SST to coral $\delta^{18}O$ varies globally; for example, west/south Pacific corals more strongly reflect salinity than those in the central/east Pacific (Russon et al., 2013). This contribution is leveraged in this study to reconstruct global tropical salinity from sites with strong salinity signals. Previous coral studies have capitalized on salinity coherence across large spatial scales to reconstruct regional salinity variability and trends (e.g., Dassié et al., 2018; Gorman et al., 2012), but coral-based reconstructions of the global tropics are rare.

Here we apply a reduced-space approach to climate field reconstruction (CFR) (Evans et al., 2002; Fritts et al., 1971; Mann et al., 1998) that has been previously used in paleoclimate research (Gill et al., 2016). We

Paleoceanography and Paleoclimatology

10.1029/2021PA004371

**Table 1**
*Salinity Data Sets Used in This Study*

| Short name | SODA2.2.4 | SODA2.1.6 | SODA3.3.1 | SODA3.4.2 | ORAS5_0 - ORAS5_4 | GODAS | EN4 | Delcroix | IAP |
|---|---|---|---|---|---|---|---|---|---|
| Full name | Simple Ocean Data Assimilation version 2.2.4 | Simple Ocean Data Assimilation version 2.1.6 | Simple Ocean Data Assimilation version 3.3.1 | Simple Ocean Data Assimilation version 3.4.2 | ECMWF Ocean ReAnalysis System 5 ensemble members 0–4 | NCEP Global Ocean Data Assimilation System | UK Met Office Hadley Centre EN4.2.1 | Delcroix SSS | Institute of Atmospheric Physics gridded ocean product |
| Type | Reanalysis | Reanalysis | Reanalysis | Reanalysis | Reanalysis | Reanalysis | Objective Analysis | Objective Analysis | Observational Reconstruction |
| Model used | POP2.0.1 | POP2.1 | GFDL CM2.5 MOMv5.1 | GFDL CM2.5 MOMv5.1 | NEMOv3.4.1 & LIM2 | GFDL MOM.v3 | - | - | CMIP5 historical simulations |
| Forcing | 20CRv2 | ERA-40 + QuickSCAT | MERRA2 + flux correction | ERA-Interim + flux correction | ERA-Interim (1979–2015), ECMWF NWP (2015-) + flux correction | NCEP R2 | - | - | - |
| Salinity observations assimilated | WOD09 | WOD09 | WOD13 | WOD13 | EN4 profiles | None | WOD13, ASBO, GTSPP, Argo + Gouretski and Reseghetti (2010) corrections | WOD09, voluntary observing ships, research cruises | WOD18 + Cheng and Zhu (2014) corrections |
| Salinity depth (m) | 5.01 | 5.01 | 5.03 | 5.03 | 0 | 5 | 5.02 | 0 | 1 |
| Spatial resolution (lat × lon) | 0.5° × 0.5° | 0.5° × 0.5° | 0.5° × 0.5° | 0.5° × 0.5° | 1° × 1° | 0.33° × 1° | 1° × 1° | 1° × 1° | 1° × 1° |
| Time span | 1871–2008 | 1958–2008 | 1980–2015 | 1980–2019 | 1979–2018 | 1980–2020 | 1900–2020 | 1950–2008 | 1940–2020 |
| Reference | Giese and Ray (2011) | Carton and Giese (2008) | Carton, Chepurin, and Chen (2018) | Carton, Chepurin, and Chen (2018) | Zuo et al. (2019) | Behringer and Xue (2004) | Good et al. (2013) | Delcroix et al. (2011) | Cheng et al. (2020) |
| Notes | | | | | Ensemble member 0 has no perturbations applied; members 1–4 have perturbations in forcings, observations, and initial conditions | Incorporates "synthetic salinity profiles" computed from the World Ocean Database; the CPC notes that "GODAS seriously underestimates salinity variability" | Relaxes to climatology when/where observations are sparse, which can affect trends and variability | Tropical Pacific (30°S–30°N) only; relaxes to climatology when/where observations are sparse | Uses model-derived spatiotemporal covariance to generate an interpolated product; sampling uncertainty is similar in magnitude to interannual variability prior to 2005; large uncertainties before 1960 |

*Note.* Monthly means are used for all data, and the time span, spatial resolution, and vertical depth of the salinity data are also given. Information given for reanalysis data includes: the climate model used; the source of atmospheric forcings (including any corrections to surface fluxes, such as heat and freshwater); and the source of salinity observations that are assimilated.

compile a network of SSS-sensitive coral $\delta^{18}O$ records, and use this network to reconstruct 20th century annual salinity anomalies in low-latitude regions where reef-building (scleractinian) corals are found (30°N–30°S), which we call the "full tropics" hereafter. We then assess the accuracy of this SSS reconstruction, with the goal of identifying avenues for method improvement and extension further into the past. In order to accomplish these goals, we address the following questions:

1. Which coral $\delta^{18}O$ records are best suited to reconstructing salinity?
2. Do all SSS data sets yield similar salinity reconstructions?
3. What 20th century SSS variability and trends are captured by coral-based reconstructions?

## 2. Methods

### 2.1. Salinity Data

We begin by compiling full tropical gridded SSS data sets that substantially overlap with coral records, requiring that the SSS data are available in 1980 or earlier. These data sets include multiple reanalysis and OA products. Table 1 describes each product, the salinity observations upon which they are based, and the challenges and opportunities associated with each.

Four members of the Simple Ocean Data Assimilation (SODA) reanalyzes were chosen, including two members of SODA version 2 and two members from version 3. SODA2.2.4 was chosen as its time span, 1871–2008, makes it a favorable and often-used candidate for coral calibration (Giese & Ray, 2011); we also include SODA2.1.6 (Carton & Giese, 2008), SODA3.3.1 (Carton, Chepurin, & Chen, 2018), and SODA3.4.2 (Carton, Chepurin, & Chen, 2018) for comparison, though these data sets are shorter (Table 1). For SODA products, ocean models are forced by near-surface variables from atmospheric reanalyzes, such as winds, air temperature, humidity, pressure, precipitation, and radiative fluxes. The underlying ocean models and forcings differ among SODA versions; recent iterations (SODA3) also introduce corrections for biases in net surface heat and freshwater flux (Carton, Chepurin, & Chen, 2018).

The European Centre for Medium-Range Weather Forecasts Ocean ReAnalysis System 5 (ORAS5) ensemble members (0–4) are also included (Zuo et al., 2019) (Table 1). These members only differ by perturbations to the initial conditions, atmospheric forcings (e.g., heat, momentum, and freshwater fluxes), and observations (derived from EN4 profiles) (Zuo et al., 2017), and are therefore highly similar to each other.

The final reanalysis data set, the National Centers for Environmental Prediction Global Ocean Data Assimilation System (GODAS) (Behringer & Xue, 2004), does not directly assimilate salinity observations, and instead computes and assimilates synthetic salinity profiles using temperature and salinity climatology from the National Centers for Environmental Information World Ocean Database (WOD) (Saha et al., 2006) (Table 1).

OA products, in contrast to reanalyzes, do not assimilate observations into climate models, theoretically circumventing biases in model physics. These products are sensitive to the number and spatial distribution of observations, however, as well as the method used to infill missing observations. OA products considered here include UK Met Office Hadley Center EN4.2.1, Delcroix, and Institute of Atmospheric Physics (IAP) SSS (Table 1). EN4.2.1 extensively quality-controls salinity profiles from WOD (Boyer et al., 2013), the Global Temperature and Salinity Profile Program (Sun et al., 2010), and Argo (Argo, 2020) to produce a gridded product that spans the full 20th century (Good et al., 2013). Another OA product, Delcroix, exclusively reconstructs near-surface ($\leq$10 m) salinity and therefore draws from a larger pool of observations, but is only available in the tropical Pacific Ocean (Delcroix et al., 2011). Both OA products relax to the climatological mean in the absence of observations. Finally, a recently released interpolated salinity product from IAP similarly draws from WOD observations (Cheng et al., 2020). However, the IAP method infills missing data by using error covariance maps derived from an ensemble of historical Coupled Model Intercomparison Project Phase 5 simulations. This Observational Reconstruction approach differs from that of EN4.2.1 and Delcroix, which infill data using an isotropic or ellipsoid function (Delcroix et al., 2011; Good et al., 2013).

These reanalysis and OA data sets are chosen to be illustrative examples, not exhaustive compilations. Further, as they often assimilate identical or near-identical data sets, such as the 2013 or 2018 iterations of the WOD (Boyer et al., 2013, 2018), they cannot be treated as truly independent estimates of salinity. Though WOD18 includes

nearly 2 million surface-only salinity observations, such observations are not the main focus of the WOD, which mainly compiles sub-surface profiles; instead, the WOD includes surface-only observations only when/where profiles are sparse (Boyer et al., 2018). To our knowledge, no gridded, global, and long-term SSS data set assimilates satellite-derived salinity observations (reviewed in N. Vinogradova et al. [2019]).

We restrict all data sets to the full tropics (30°S–30°N). The SSS data are then averaged from April to the following March (i.e., the "tropical year") to avoid splitting ENSO events between years (Evans et al., 2002). Only tropical years with 12 months of data are included to mitigate biases introduced by incomplete years. This annual mean calculation can potentially smooth lagged relationships of salinity with subannual-to-interannual climate variability (e.g., salinity at sites in the South Pacific can lag ENSO by as much as 7 months [Kilbourne et al., 2004]), so we caution that interannual variability may be underestimated in comparison to decadal-to-multidecadal variability and trends. Where needed, data are converted from absolute (g/kg) to practical (PSU) salinity using the Thermodynamic Equation of Seawater (IOC et al., 2010). Finally, we subtract the temporal mean over the 1980–1990 reference period, chosen as the period of overlap between all SSS data sets and most coral records, to compute SSS anomalies (SSSa).

### 2.2. Coral Data and Calibration

Coral $\delta^{18}O$ data used in this study are compiled from the Iso2K database (Konecky et al., 2020). All coral records are screened based on several criteria, such that all records: (a) are located within the global tropical-subtropical oceans (30°S–30°N); (b) have a temporal resolution of annual or higher; (c) overlap and extend the SSS calibration period starting in 1970 (i.e., each record begins in 1960 or earlier and ends after 1980, such that there is at least 10 years of overlap and pre-instrumental coral data). We include several additional records that meet these criteria, including an updated version of the Fonoifua Island, Tonga record (TF1 in the original publication; Iso2K ID CO18DATO01A) (Dassié et al., 2018), one record from Ha'afera Island, Tonga (TH1 in the original publication) (Linsley et al., 2017), and two records from the Lombok Strait, Indonesia (Murty et al., 2018) (Table S1 in Supporting Information S1).

For each location, we calibrate annual coral $\delta^{18}O$ with annual SSS over the calibration interval (defined to begin in 1970, when observations are more frequent (Figure 1), and continuing to the most recent date of each coral record). First, we calculate the annual, tropical-year mean for each sub-annually resolved coral record. Annually resolved records are assumed to span the tropical year. We then calibrate each coral record to SSS using weighted least squares (WLS) regression, a linear regression method that accounts for uncertainty in both the independent and dependent variables (Thirumalai et al., 2011). We perform this calibration separately for each SSS data set considered in this study, and for each $\delta^{18}O$ record at sites where multiple records are available. A coral record is only calibrated if it overlaps with an SSS grid cell, which eliminates some near-shore coral records. We also require an overlapping sample size of at least 5 years. Though this flexible calibration period could preferentially include more recent coral records (for which the calibration period is longer and more likely to produce significant relationships with SSS), this approach maximizes the salinity information obtained by the network of available records compared to calibration over a common period (e.g., 1980–1990). Finally, we evaluate uncertainty in the calibration equation for each coral record and SSS data set by using *K*-fold cross validation (see Supporting Information S1).

WLS regression requires uncertainty estimates for both coral $\delta^{18}O$ and SSS. For coral $\delta^{18}O$, we use the $1\sigma$ analytical uncertainty. Because all of the reanalysis and some of the OA SSS data sets lack uncertainty estimates, we use $1\sigma$ SSS error from the EN4.2.1 gridded product for all SSS data sets except Delcroix, which includes its own uncertainty calculations (note that IAP SSS error estimates are not publicly available as of April 2021, so EN4.2.1 error is used for IAP as well). Many SSS data products incorporate similar or identical observations (especially the WOD) (Table 1), making EN4.2.1 uncertainties a reasonable choice in the absence of individualized uncertainty data sets.

We remove any coral records with a $\delta^{18}O$-SSS calibration $p > 0.1$; this $p$-value was chosen to buffer against the impacts of small sample sizes in calibrations with shorter SSS data sets (e.g., for ORAS5, mean calibration $n = 17$) to maximize the salinity information obtained from the network of available coral records. We then apply the calibration equation to convert the remaining coral $\delta^{18}O$ records to SSS. If there are multiple records for each model grid cell, we then composite SSS at each site by Z-scoring each SSS reconstruction, averaging these

Z-scores, then converting this composite Z-score to SSS using the mean and standard deviation of the SSS reconstructions during their period of overlap. We then calculate SSSa relative to the reference period for each grid cell.

### 2.3. Reconstruction Method

The reduced-space reconstruction method used here is adapted from the method described by Gill et al. (2016) (see Gill Figure 3 for a visual explanation of the method). The procedure for each SSSa data set is as follows:

**EOF Analysis of SSS Data Products**

1. SSSa is interpolated to 2° × 2° spatial resolution to speed computations in step 3 (results [not shown] are similar when the original resolution is used). The interpolated SSSa is then reshaped from three dimensional (latitude × longitude × time) to two dimensional (time (length $N$, the number of years of the full SSSa data set) × number of grid cells with SSSa data (length $G$)), producing the matrix $\mathbf{X}_{full}$.
2. The covariance matrix, $\mathbf{C}_{full}$, has dimensions $G \times G$, and is computed from $\mathbf{X}_{full}$ using the NumPy cov function in Python (Harris et al., 2020).
3. $\mathbf{C}_{full}$ is decomposed into orthogonal space-time components (hereafter "modes") by performing singular value decomposition on $\mathbf{C}_{full}$ using the SciPy linalg.svd package in Python (Virtanen et al., 2020):

$$\mathbf{C}_{full} = \mathbf{U}_{full}\mathbf{\Lambda}_{full}\mathbf{U}_{full}^{T}. \quad (1)$$

$\mathbf{U}_{full}$ is a matrix of eigenvectors (i.e., the spatial loadings, or EOFs, of each mode). $\mathbf{U}_{full}^{T}$ is the transpose of $\mathbf{U}_{full}$, and $\mathbf{\Lambda}_{full}$ is a matrix with the eigenvalues, $\lambda_{full}$, on the diagonal; these eigenvalues can be used to calculate the fraction of the total variance described by each mode. $\mathbf{U}_{full}$, $\mathbf{\Lambda}_{full}$, and $\mathbf{U}_{full}^{T}$ all have dimensions $G \times G$. The temporal evolution of each EOF is termed the "principal component" (PC). The matrix of principal components, $\mathbf{A}_{full}$, has shape $N \times G$, and is calculated by multiplying the reshaped SSSa matrix by the eigenvectors:

$$\mathbf{A}_{full} = \mathbf{X}_{full}\mathbf{U}_{full} \quad (2)$$

Note that the signs of these eigenvectors (and thus PCs) are arbitrary, and can be inverted as needed to be consistent with the temporal evolution of real modes of climate variability (such as ENSO).

**Coral Site EOF Analysis and Regression Model Development**

4. A matrix is formed of a subset of the high-resolution SSSa grid cells (i.e., not interpolated to 2°) for each data product that include only the locations of coral proxies. This matrix, $\mathbf{X}_{subset}$, has dimensions $N \times P$, where $P$ is the number of grid cells with coral proxy sites. Repeat steps 2 and 3 with $\mathbf{X}_{subset}$. This process yields: the EOFs $\mathbf{U}_{subset}$ (dimensions $P \times P$); principal components $\mathbf{A}_{subset}$ (dimensions $N \times P$); and, finally, the eigenvalues $\lambda_{subset}$ of the subset field.
5. Because the variance in a full-field mode may capture the variance of a combination of subset-field modes, multiple linear regression is used to reconstruct each full-field PC using a combination of the leading subset-field PCs as predictors (i.e., the consecutive subset-field PCs that together explain at least 75% of the cumulative variance [Text S2 in Supporting Information S1]). Regressions using all possible combinations of these subset-field PCs are evaluated using the Bayesian Information Criterion (BIC), and the combination that yields the lowest BIC is used. This process yields regression equations for the leading $y$ full-field modes using the $x$ retained limited-field PCs. The $r^2$ value (adjusted for the number of predictors [Miles, 2014]) of each multiple linear regression is then calculated. Only the leading consecutive full-field modes that produce an adjusted $r^2 \geq 0.2$ are explicitly reconstructed (see Supporting Information S1).
6. A matrix is formed of coral SSSa data (composited for each site), $\mathbf{F}$, with dimensions $L \times P$, where $L$ is the time span of the coral matrix. We infill missing data within each site with 0 (i.e., the mean during the SSSa reference period).

**Climate Field Reconstruction**

7. For each year $l$ in the time span $L$ of the coral matrix, reconstruct the subset-field principal components, $A_{subset\_R\_l}$ (dimensions $1 \times P$); where applicable, variables are denoted $R$ for "reconstructed":

$$A_{subset\_R\_l} = F_l \mathbf{U}_{subset} \quad (3)$$

We then find the leading reconstructed full-field principal components, $A_{full\_R\_l}$, using $A_{subset\_R\_l}$ and the regression equations found in step 5. $A_{full\_R\_l}$ is a row vector of length $y$; the temporal mean of the remaining full-field PCs is then used to fill the remaining space in $A_{full\_R\_l}$ (i.e., extending $y$ to length $G$) so that the spatial expression of these combined principal components can be calculated. Finally, these reconstructed PCs are converted to reconstructed full-field SSS anomalies for each year $l$:

$$X_{full\_R\_l} = A_{full\_R\_l} \mathbf{U}_{full} \quad (4)$$

The calculation of $X_{full\_R\_l}$ (dimensions $1 \times G$) is then repeated for each year $l$ in which coral proxies are available.

8. After looping through step 7 for each year, the results are ultimately compiled into matrix $\mathbf{X}_{full\_R}$ (dimensions $L \times G$). This matrix is then reshaped to produce the three-dimensional (latitude × longitude × $L$) CFR of SSSa.
9. Finally, we truncate the CFR to the period in which at least 50% of the maximum number of screened coral sites for each SSS data set are available. Below this threshold, more than half of the sites are assigned reconstructed SSSa values of zero, and we observe that the principal components similarly relax toward the mean (data not shown). This process ultimately yields a coral-based CFR for each SSSa data set.

We compute the full- and subset-field modes for all SSA data sets. We then evaluate the leading EOFs and PCs of each data set for evidence of unphysical behavior (e.g., unrealistic temporal trends or visual evidence of the sparse observation network influencing spatial patterns) before considering them for CFR.

### 2.4. Error Assessments

We perform error assessments of each CFR over the full period of overlap among reconstructions and SSS data (1980–1997). We caution that assessments over this period may not hold true over longer time scales, but this is an unavoidable limitation of short salinity observations relative to those of other climate variables, such as SST. We considered calibration-validation analyses for both coral $\delta^{18}$O-SSS calibration and for comparing the $CFR_{coral}$ to SSS data. However, the period of overlap between all SSS data sets and most coral records is too short to split into two sufficiently sized intervals: SSS data typically begins in 1980, and most coral records end in the mid-1990s, such that the 50% threshold used to truncate the CFR occurs around 2000 CE. This limited sample size (<10 years for each interval) precludes an informative out-of-sample validation approach.

We compare the $CFR_{coral}$ from each SSS data set to the SSS data set used to reconstruct it (e.g., IAP SSSa compared to SSSa from the IAP $CFR_{coral}$), hereafter the "respective SSS" of each CFR, by computing the Anomaly Correlation statistic (AC). The AC is essentially the product-moment correlation coefficient ($r$-value) between reconstructed and original SSSa computed for each grid cell and then spatially averaged (Cook et al., 2011; Wilks, 2006). We also map the long-term mean $CFR_{coral}$-SSS difference over the period of overlap. This process allows the examination of spatial or temporal biases in each $CFR_{coral}$ compared to its respective SSS data set.

To better assess the sources of error in the climate field reconstructions, we generate an "SSS observation-based CFR" from each SSS data set ("$CFR_{SSS}$"). We compute each $CFR_{SSS}$ by following the steps 1–5 in Section 2.3 used to generate each $CFR_{coral}$. In step 6, rather than generating matrix $\mathbf{F}$ from coral data, we create this matrix using the SSS from the grid cells of the included coral data. This matrix, $\mathbf{F}_{SSS}$, has dimensions $N \times P$. We then complete the CFR (steps 7–9) using $\mathbf{F}_{SSS}$ instead of $\mathbf{F}$. In a sense, this approach produces a "best case" CFR, one in which the coral records from each site perfectly reflect SSS and thus introduce no additional error to the recon-

struction. We then repeat the $CFR_{coral}$ error assessments using $CFR_{SSS}$. By comparing $CFR_{SSS}$ to its respective SSS data set, we can quantify the uncertainties that result from a combination of: (a) the number and location of coral sites, and (b) the CFR method, such as the number of modes that are explicitly reconstructed, and the regression between the full- and subset-field PCs. We also compare $CFR_{coral}$ to $CFR_{SSS}$ to assess the additional error that may result from the coral records. Sources of such error may include uncertainty in the $\delta^{18}$O-SSS calibration slope and intercept, contribution of SST to coral $\delta^{18}$O, age model uncertainty, and non-climatic $\delta^{18}$O variability due to growth-related ("vital") effects (McConnaughey, 1989).

### 2.5. Climate Analyses

To identify significant long-term trends, each reconstruction is subset to a common period when most coral records are available (1900–1990). Ordinary least squares (OLS) regression coefficients are then computed and evaluated for significance (after Santer et al. [2000]). These trends are then compared among reconstructions. We compare the response of reconstructed and instrumental SSSa fields to ENSO events using the Niño3.4 index (ERSSTv5 over 5°S–5°N, 170°–120°W; detrended by subtracting mean SST over 20°S–20°N). We further compare the Niño3.4 index to the coral reconstruction of the SSS mode that most strongly reflects ENSO. We also evaluate regressions of reconstructed salinity with the Interdecadal Pacific Oscillation (Henley et al., 2015), Atlantic Multidecadal Oscillation (Trenberth & Shea, 2006), and Indian Ocean Dipole (Saji et al., 1999), all computed using ERSSTv5 (Huang et al., 2017). We note that computing the IOD index using ERSSTv5 enables comparisons over the full 20th century, but may reduce the magnitude of inferred IOD events compared to shorter and higher-resolution SST products (Abram, Hargreaves, et al., 2020). The Atlantic Multidecadal Oscillation (AMO) index is smoothed with a 10-year running mean, and all climate indices are computed over the tropical year. We compare these salinity regression maps with those of reanalysis-based precipitation minus evaporation ("P−E") data (NOAA/CIRES/DOE 20th Century Reanalysis version 3, Slivinski et al., 2021), but caution that P−E and SST observations, like salinity observations, are scarce for most ocean basins during much of the 20th century.

### 2.6. Assumptions

The EOF analysis approach to CFR requires several key assumptions. The first assumptions arise from the SSS data: we assume that the SSS data sets span enough time to accurately capture the leading modes of variability, and that SSS modes result from real SSS variability and are not an artifact of changing number, location, and/or method of salinity observations through time. Other assumptions are more fundamental: this CFR method assumes that the leading modes of variability over the period of EOF computation remain the dominant modes of variability over the reconstruction period. We further assume a multivariate, linear relationship between the PCs of full SSS field and the subset field.

The final assumptions arise from the coral data. We assume that the coral $\delta^{18}$O-SSS calibration is valid over the reconstruction period. This calibration may be affected by nonlinearities in local seawater $\delta^{18}$O-SSS relationships that cannot be constrained without in situ seawater isotope measurements (Legrande & Schmidt, 2011; Stevenson et al., 2018). In addition, we assume that the contribution of SST to coral $\delta^{18}$O does not meaningfully affect our SSS reconstructions. A paired geochemical approach potentially avoids this assumption by subtracting a Sr/Ca-derived SST signal from coral $\delta^{18}$O to isolate a seawater $\delta^{18}$O (and therefore salinity) signal (Cahyarini et al., 2008; Ren et al., 2002). However, we did not apply this approach in this study for three reasons. First, the number of paired Sr/Ca-$\delta^{18}$O records is small compared to the number of $\delta^{18}$O-only records. Second, SST-SSS covariance can bias paired Sr/Ca-$\delta^{18}$O salinity reconstructions. Where covariance is strongly negative (i.e., at many of our coral sites [Russon et al., 2013]), the $\delta^{18}$O-SST calibration slope is anomalously steep; as a consequence, this method may yield reconstructions not of total seawater $\delta^{18}$O, but of the small fraction of the seawater $\delta^{18}$O signal that varies independently of SST (Cahyarini et al., 2008). Third, compounding errors (Sr/Ca-SST and $\delta^{18}$O-SST regressions, and analytical uncertainties of Sr/Ca and $\delta^{18}$O) can further weaken signal-to-noise ratios. A seawater $\delta^{18}$O reconstruction method that accounts for SST-SSS covariance could improve the CFRs in this study. In the absence of such a method, we use unpaired coral $\delta^{18}$O, leveraging the SST-SSS covariance that can amplify salinity signals, and caution that the SST contribution could be a source of uncertainty beyond the calibration period.

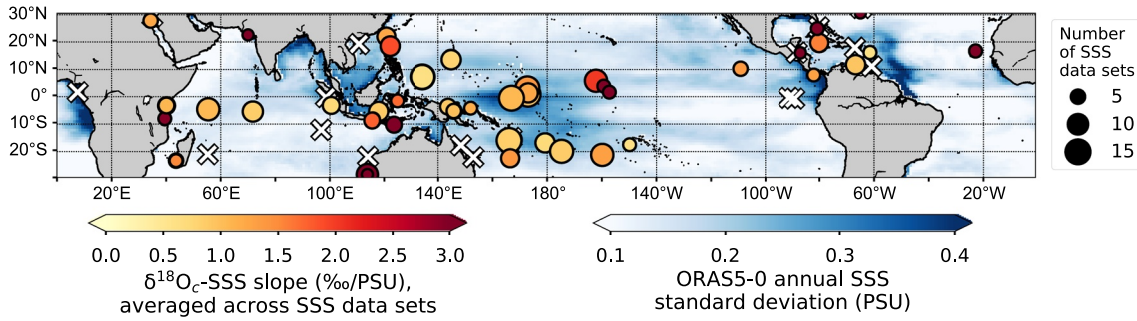


**Figure 2.** Calibration slope (colored circles) between coral $\delta^{18}O$ and sea surface salinity (SSS) for each coral record, averaged across SSS data sets. All data sets (e.g., Delcroix, Global Ocean Data Assimilation System, and EN4.2.1) are included; for individual calibrations, see Figure S2 in Supporting Information S1. The mean slope excludes any calibrations that fail the screening criteria for sample sizes and significance given in the Methods. Circle size corresponds to the number of SSS data sets for each coral record that yield a calibration that passes the screening criteria (larger size = significantly correlated with more SSS data sets). White X's denote sites where no calibration passes the screening criteria. Background shading shows the standard deviation of annual SSS (ORAS5-0).

## 3. Results and Discussion

### 3.1. Coral Record Calibration

Of the 74 coral $\delta^{18}O$ records considered, between 16 and 37 pass the screening criteria for inclusion in the CFR, depending on the specific SSS data set (Figures S1 and S2 in Supporting Information S1). Data sets with longer overlaps with coral records (SODA2.2.4 and 2.1.6, EN4.2.1, IAP, and Delcroix) generally include more coral sites than shorter SSS data sets, likely due to larger sample sizes (Figure S2 in Supporting Information S1). Few records from the central/eastern equatorial Pacific, Atlantic, and Caribbean Sea pass the screening criteria. Those that do generally show steeper $\delta^{18}O$-SSS slopes (which translates to a small coefficient when converting $\delta^{18}O$ to SSS) (Figure 2 and Figure S2 in Supporting Information S1). Some nearshore sites (e.g., the Great Barrier Reef) are not significantly correlated with any SSS data sets. This may result from sub-grid-scale variations in SSS due to runoff, river input, and local ocean circulation. Comparing our regressions with published $\delta^{18}O$-SSS calibrations for individual sites, we find that WLS $\delta^{18}O$-SSS slopes are steeper than those of OLS. This difference is expected because accounting for SSS uncertainties in WLS regressions typically increases the magnitude of regression slopes. Nonetheless, WLS produces SSS reconstructions with consistently smaller errors when compared to OLS-based SSS reconstructions (Table S2 in Supporting Information S1). For sites that pass the calibration screening criteria, *K*-fold cross validation (see Supporting Information S1) shows that coral-based SSS reconstructions for each record have a median uncertainty of 0.13–0.24 PSU (RMSE) compared to the SSS time series from the nearest grid cell (Figure S3 in Supporting Information S1). Uncertainty is lowest for IAP and highest for SODA3 members.

Sites with significant correlations with the most SSS data sets cluster in the ITCZ and SPCZ. In these regions, salinity variance, and therefore $\delta^{18}O_{sw}$ variance, is high (Figure 2), so coral $\delta^{18}O$ variability is expected to strongly reflect $\delta^{18}O_{sw}$ and its covariance with SST (Russon et al., 2013). Warmer and fresher conditions co-occur in most of these regions, strengthening the significance of coral $\delta^{18}O$-SSS regressions (Russon et al., 2013). In other regions, such as the central/eastern Pacific and southern Indian Ocean, few records pass $\delta^{18}O$-SSS significance testing. In these regions, SSS and SST may not constructively covary, and sometimes even destructively covary, with warmer and saltier conditions coinciding (Russon et al., 2013). This may weaken $\delta^{18}O$-SSS regressions below the threshold of significance, especially in regions where overall salinity variance is low. Therefore, the distribution of coral records that are significantly related to salinity is in agreement with expected coral $\delta^{18}O$ behavior, based on spatio-temporal patterns of SST and $\delta^{18}O_{sw}$ variability.

### 3.2. Modes of Variability in SSS Data Sets

A prerequisite to reduced-space climate reconstruction is identifying the leading modes of variability to reconstruct. We evaluate the leading modes of variability in the SSS data sets to determine their suitability for reconstruction, and any discrepancies in these modes among SSS data products would have important implications for coral-based climate field reconstructions. This evaluation is not intended to comprehensively assess or interpret

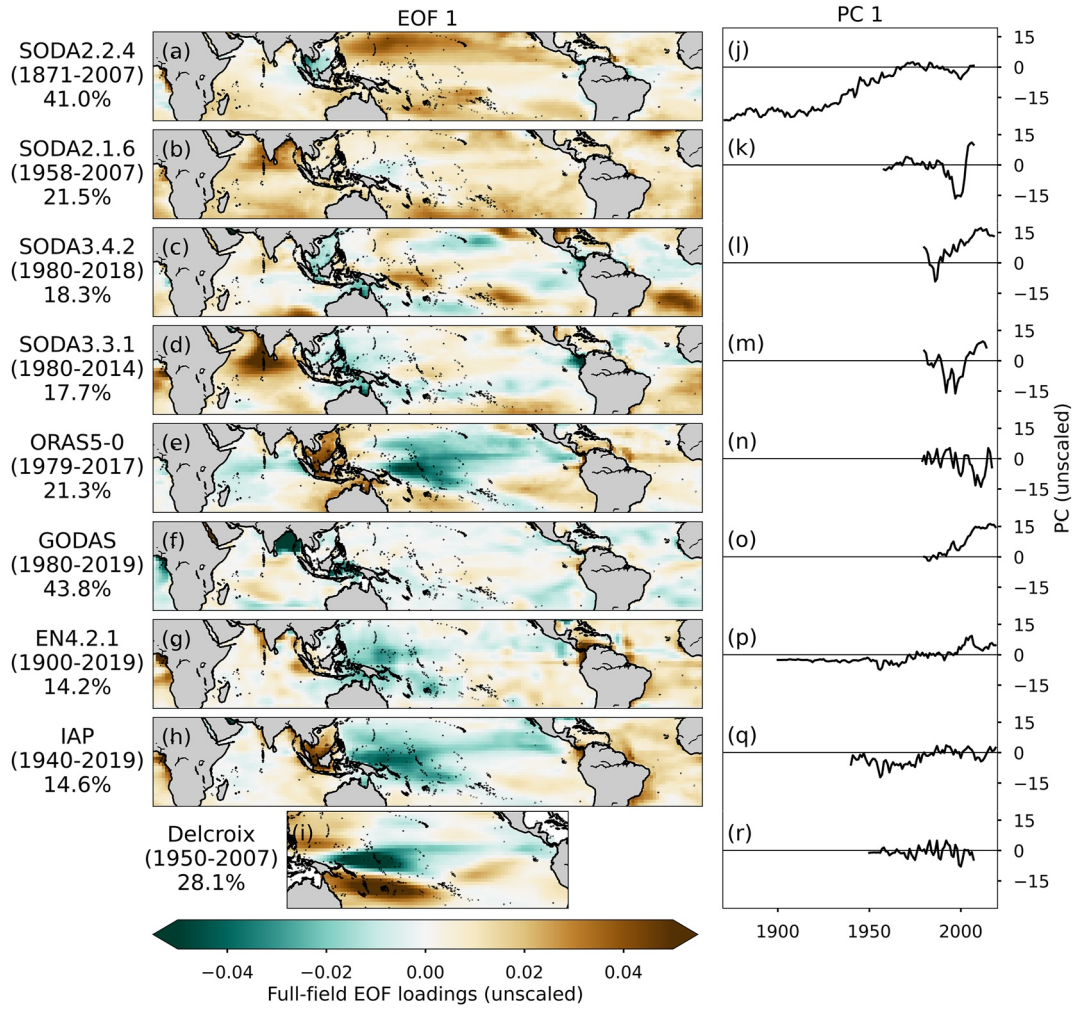


**Figure 3.** The spatial (EOF; left column) and temporal (PC; right column) pattern of the leading mode of variability for each sea surface salinity data set considered in this study. EOFs and PCs are unscaled, and the signs of the loadings are arbitrary. ORAS5-1 through ORAS5-4 are similar to ORAS5-0 and are not shown. The time span (in tropical years) of each salinity data set, and the percentage of total salinity variance explained by the leading mode, are given at left.

the climatic significance of salinity modes of variability. Instead, we screen for unphysical variability that could be an artifact of the evolving observation network, infilling method (for OA), or model-based climate forcings and flux corrections (for reanalyzes), which would preclude their use for paleoclimate reconstruction. Overall, the spatial and temporal patterns of the leading modes are inconsistent among SSS data sets (Figures S4 and S5 in Supporting Information S1). These discrepancies persist even if the data are subset to the common period before computing EOFs (1980–2008; Figures S6 and S7 in Supporting Information S1), and exemplify the uncertainties that can result from sparse salinity observations over the 20th century (Figure 1).

We evaluate the leading modes of variability computed from the full time span of each SSS data set, and show the first mode (EOF1 and PC1) for comparison among data sets (Figure 3). SODA2 EOF1 loads in the same direction across nearly the entire tropics (Figures 3a and 3b). In SODA2.2.4, the leading mode is a long-term trend (Figure 3j), which is less clear during the shorter time span of SODA2.1.6 (Figure 3k). The fact that this nearly pan-tropical pattern is absent from all other SSS data sets, including more recent SODA versions (Figures 3c and 3d) indicates that this mode is likely non-climatic in origin. Flux corrections were not implemented in SODA2, and could account for the unrealistic trend in these members; by comparison, evaporative fluxes in SODA3 were corrected by up to +2 mm/day (Carton, Chepurin, & Chen, 2018; Carton, Chepurin, Chen, & Grodsky, 2018). Therefore, we do not use SODA2 for coral reconstructions.

We exclude SODA3 and GODAS from reconstructions for similar reasons. SODA3 and GODAS EOF1 show weak regional spatial coherence compared to other data sets (Figures 3d and 3f). In addition, SODA3.4.2 and SODA3.3.1 EOF1 are highly dissimilar despite having nearly identical methods (Figures 3c and 3d, Table 1), indicating that these EOFs are highly sensitive to the surface forcings used in these reanalyzes. SODA3 members are also excluded because the ability of the subset field to reconstruct the full-field ENSO mode (EOF3, not shown) is below the $r^2$ cutoff of 0.2, and is therefore not explicitly reconstructed. GODAS is precluded from reconstructions as it does not directly assimilate salinity observations, resulting in spatially incoherent EOFs that do not resemble those of any other data sets considered in this study (Figure 3f).

Several OA data sets also show evidence of non-climatic artifacts. EN4.2.1 and Delcroix SSS relax to the long-term climatology in the absence of observations, which impacts the assessment of variability and trends. This bias is visible as a dampening of PC1 variability before observations are widespread (approximately 1970 CE) (Figures 3p and 3r), and as unusually strong loadings in locations with frequent observations (e.g., the TAO array is visible in EOF1 of EN4.2.1; Figure 3g).

The remaining data sets include IAP and the ORAS5 ensemble. These data sets show no obvious impacts of the composition of observations (i.e., changes in the frequency, type, and/or location through time). For example, the leading mode of IAP (Figures 3h and 3q) is similar to that of EN4.2.1 (Figures 3g and 3p), but with no visible variability damping before 1970, and with greater regional spatial coherence compared to EN4.2.1 due to differences in IAP's infilling method for sparse observations. IAP EOF1 shows a spatial pattern that resembles salinity trends during the mid-to-late 20th century seen in previous studies (Cheng et al., 2020; Durack et al., 2012; Skliris et al., 2014), and PC1 shows strong multidecadal variability or a trend (Figures 3h and 3q). Because ORAS5-0 spans a shorter time period than IAP, IAP and ORAS5-0's modes are shuffled and/or intermixed relative to each other. For example, ORAS5-0 PC1 is characterized by interannual rather than multidecadal variability (Figure 3n), as expected when computing EOFs over short time spans. Nonetheless, ORAS5-0 PC1 is significantly correlated with both IAP PC1 and PC2 ($r = 0.79$ and 0.84, respectively; autocorrelation-adjusted $p < 0.05$, after Bretherton et al. (1999); Figure S4 in Supporting Information S1). ORAS5 PC1 and IAP PC2 are not only strongly correlated, but their EOFs are especially similar, with the strongest negative loadings in the western equatorial Pacific (Figures 3e and 3n; Figure S4 in Supporting Information S1). This region has notably high interannual SSS variability, which is linked to ENSO events (Chi et al., 2022; Delcroix et al., 2011; Qi et al., 2019; Singh et al., 2011); indeed, ORAS5-0 PC1 and IAP PC2 are both significantly correlated with the Nino3.4 index ($r = 0.73$ and 0.77, respectively; adjusted $p < 0.05$). Ultimately, the ORAS5 ensemble and IAP provide one example each of reanalysis and OA-based SSS data sets that we retain for use in coral-based salinity reconstructions.

### 3.3. Salinity Field Reconstruction

The IAP and ORAS5 coral-based SSS reconstructions range from 115 to 131 years in length (dependent on the availability of coral records used in the reconstruction), and all reconstructions span the period 1890–1999. We generate these CFRs by reconstructing the leading 2–4 full-field modes (Figure S8 in Supporting Information S1), for which which at least 20% of the variance are explicitly reconstructed by corals (i.e., $r^2 \geq 0.2$; Figure S9 in Supporting Information S1). Together, these reconstructed modes explain at least 30% of the total subset-field and full-field variance of each SSS data set. Sensitivity analyses demonstrate that including additional modes by lowering the $r^2$ threshold to zero (i.e., reconstructing more of the total variance, but with modes that are not well reconstructed by the corals) only marginally increases the AC scores (see Supporting Information S1). AC scores plateau at $r^2 \geq 0.2$; therefore, our approach reconstructs the greatest variance explained while maintaining information from the coral proxies.

### 3.4. Sources of Uncertainty

A comparison of the long-term mean difference between each $CFR_{coral}$ and the SSS data product used to reconstruct it shows biases in each coral-based CFR of up to 0.36 PSU (Figures 4a and 4e). The same analyses between $CFR_{SSS}$-SSS (Figures 4b and 4f) are nearly indistinguishable from $CFR_{coral}$-SSS. These same findings are borne out by the spatial mean RMSEs through time (Figures 4d and 4h): for both IAP and ORAS5, $CFR_{coral}$-SSS and $CFR_{SSS}$-SSS are nearly identical, and the RMSEs between the two CFRs is much smaller. These analyses indicate

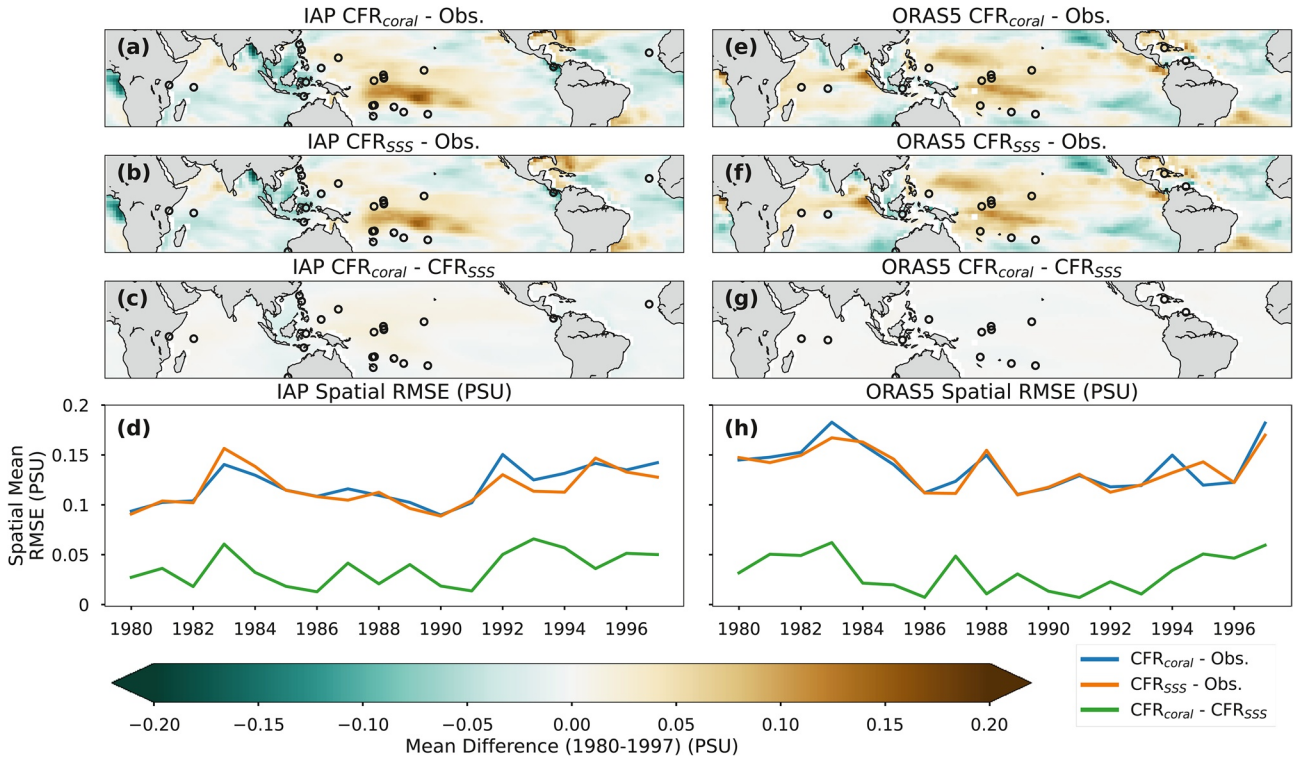


**Figure 4.** Long-term mean difference over the common period (1980–1997) between: each $CFR_{coral}$ and the sea surface salinity (SSS) data product used to reconstruct it (a and e); $CFR_{SSS}$ and the SSS data product used to reconstruct it (b and f); and $CFR_{coral}$ and $CFR_{SSS}$ (c and g). The time series (d and h) show the spatial mean RMSE between each $CFR_{coral}$ and its respective SSS (blue), $CFR_{SSS}$ and its respective SSS (orange), and $CFR_{coral}$ and $CFR_{SSS}$ (green). Results are shown for Institute of Atmospheric Physics and for the ensemble mean of Ocean ReAnalysis System 5.

that discrepancies between coral-based reconstructions and observations during the period of overlap largely arise from the CFR method and the number/location of coral proxy sites, not from an inability of the coral $\delta^{18}O$ network to capture salinity variability (or from shortcomings in the coral calibration method).

The Anomaly Correlations (AC) between pairs of data sets produce similar results (Figure 5). SSS data sets show strong agreement within the ORAS5 ensemble (median AC = 0.85), but substantially weaker agreement between ORAS5 and IAP SSS (median AC = 0.33) (Figure 5). A similar pattern is shown by comparisons among coral CFRs, with weaker agreement for IAP-ORAS5 comparisons than within ORAS5 members (Figure 5; median AC = 0.55 and 0.91, respectively). These results indicate that disagreement among salinity data sets is a significant source of uncertainty in the reconstructions as well. Similar disagreements have complicated paleoclimate reconstructions of SST (Emile-Geay et al., 2013a). In contrast, when each $CFR_{coral}$ is compared to the SSS data used to generate it, the resulting ACs are virtually identical to $CFR_{SSS}$-SSS ACs (median AC = 0.26 and 0.28, respectively) (Figure 5, right two columns). Again, these results illustrate that non-salinity-related coral variability is a small source of error when compared to uncertainties resulting from discrepancies among SSS data sets; $CFR_{SSS}$-SSS comparisons indicate that methodological uncertainties and the distribution of coral sites contribute to disagreements as well.

### 3.5. Interannual Variability

Both coral-based reconstructions show strong salinity responses to ENSO, with freshening in the central-western Pacific and salinification in the Maritime Continent during El Niño events (Figure 6). These results are consistent with the notably high interannual signal-to-noise ratios in the central-western Pacific, which are less than 1 (noise-dominated) elsewhere in the global tropics (Balmaseda et al., 2015). Fortunately, this region also overlaps with the area of best coverage by coral records (Figure 2). This overlap likely explains why ENSO is well reconstructed by coral records (Figure 6). The ability to capture ENSO is quickly degraded before these central-western Pacific records are available (not shown); for example, the Tarawa $\delta^{18}O$ record ends in 1894

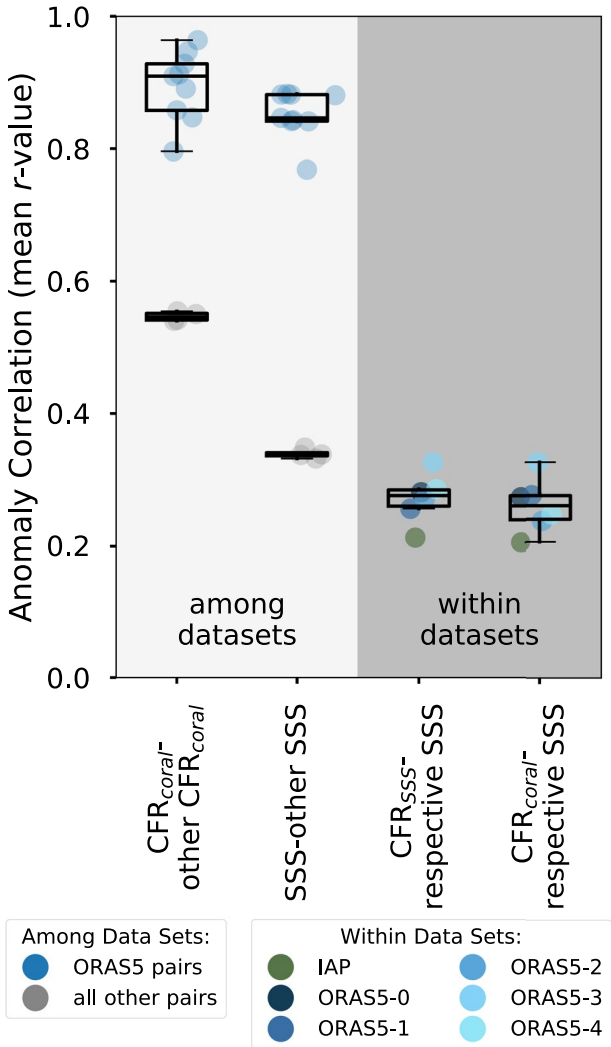


**Figure 5.** Agreement between pairs of spatiotemporal sea surface salinity (SSS) data sets and reconstructions for the common period of 1980–1997, evaluated using the Anomaly Correlation statistic (AC). Higher AC values denote greater similarity. "$CFR_{coral}$-other $CFR_{coral}$" compares coral-based CFRs generated using a variety of SSS datasets (e.g., compares the IAP-based $CFR_{coral}$ to that based on ORAS5-0). Comparisons between ORA ensemble members (e.g., ORAS5-1 $CFR_{coral}$ compared to ORAS5-2 $CFR_{coral}$) are colored in blue, and IAP-ORAS5 comparisons are colored gray. "SSS-other SSS" compares the reanalysis SSS datasets to other SSS datasets (e.g., Institute of Atmospheric Physics SSS compared to ORAS5-0 SSS); again, comparisons among ORA ensemble members are colored in blue. "$CFR_{SSS}$-respective SSS" compares the CFR created using SSS data to the SSS data set used to reconstruct it. "$CFR_{coral}$-respective SSS" is similar, except that the final coral-based CFR is used.

(Table S1 in Supporting Information S1). Both IAP and ORAS5 $CFR_{coral}$ (Figures 6c and 6d) show weaker ENSO sensitivity than their respective SSS data sets (Figures 6a and 6b); overall, ORAS5 sensitivity to ENSO (Figures 6b and 6d) is stronger than IAP (Figures 6a and 6c) in both the original data sets and coral reconstructions. Nonetheless, the principal components of SSS which strongly reflect ENSO variability (IAP PC2 and ORAS5 PC1; see Section 3.2) are significantly correlated with the Nino3.4 index in both coral CFRs ($r = 0.57$ for ORAS5-0 and 0.65 for IAP, autocorrelation-adjusted $p < 0.05$) (Figure 6e).

We also examine interannual variability in coral CFRs in several key regions, including the western equatorial Pacific, central/eastern Pacific, and portions of the IPWP and SPCZ (Figure 7). In the western equatorial Pacific, which is especially sensitive to ENSO, reconstructed SSSa are significantly correlated with their respective SSS data sets (Figure 7a). Similar results emerge from the SPCZ (Figure 7c), which also has high interannual SSS variability (Figure 2), and from the central/eastern Pacific in the ITCZ region, which has lower interannual SSS variability but is nonetheless sensitive to ENSO (Figures 6a and 6b). The IPWP is the exception to this pattern, where interannual variability is high, but correlations of reconstructed SSSa with their respective SSSa data sets are much weaker (Figure 7b). Though multiple coral records pass screening criteria in the IPWP region, none of these records are located within the South China Sea (Figure 2), which comprises a large portion of this region. For 3 of the 4 regions examined, we find that ORAS5 reconstructions yield stronger correlations with observations than do IAP reconstructions (Figure 7), which is consistent with the stronger salinity regression slopes with ENSO seen in ORAS5 compared to IAP (for both reconstructions and the original SSS data sets; Figure 6). Overall, we find that the coral CFRs yield more accurate interannual salinity reconstructions in regions that are well-represented by coral records, and where interannual variability is high.

Coral-based SSS reconstructions also capture the spatial patterns of interannual variability associated with the IOD, with salinification in the eastern Indian Ocean and freshening in the west during positive IOD events (Figure 9). Beyond the Indian Ocean, the IOD spatial pattern resembles that of El Niño, which is consistent with the tight coupling of the IOD with ENSO highlighted in previous studies (Abram, Wright, et al., 2020).

Though we interpret salinity patterns largely in terms of changes in precipitation and evaporation, other factors can influence salinity as well. For example, a salinity anomaly can be advected far from the precipitation or evaporation anomaly that caused it. We observe such circulation influences across time scales, from interannual (Figure 6) to multidecadal (Figure 8). For example, during El Niño events, the Pacific North/South Equatorial Currents (NEC, approximately 15°N; SEC, approximately 2°N) both advect unusually fresh water from the central Pacific westward; the North Equatorial Countercurrent (NECC; approximately 7°N) advects unusually salty water in the IPWP eastward; finally, upwelling of the Equatorial Undercurrent (EUC; 0°N) weakens, causing surface salinification in the eastern Pacific (Figure 6a). Similar fingerprints of advection are seen in long-term trends (Figure 8). Such advection, as well as mixing, could homogenize or dampen salinity anomalies. Nonetheless, these processes also spatially smooth and spread a salinity anomaly over a wide geographic area, making such anomalies easier to detect with a limited coral and observational network. In this way, smoothing of salinity anomalies via advection and mixing can potentially aid in the detection of long-term changes within sparse observational networks.

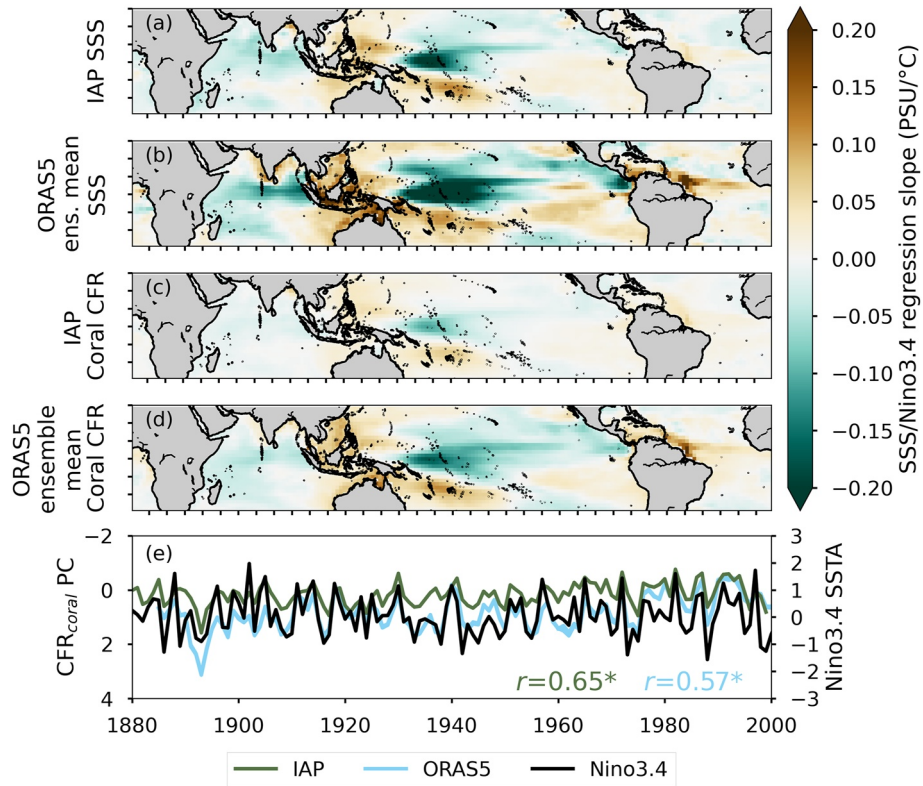


**Figure 6.** Response of sea surface salinity (SSS) to El Niño-Southern Oscillation (ENSO) events. (a and b) The linear regression slope of SSS with the Niño3.4 index (ERSSTv5, detrended by subtracting mean sea surface temperature [SST] over 20°S-20°N) for Institute of Atmospheric Physics (IAP) (a) and the Ocean ReAnalysis System 5 (ORAS5) ensemble mean (b) SSS data products. (c and d) The linear regression slope of the coral CFR with the Niño3.4 index for IAP (c) and the ORAS5 ensemble mean (d). (e) Reconstructions of the PC for each SSS data product that best reflects ENSO events, compared to Niño3.4 SST anomalies (black line). Each PC is scaled by dividing by the square root of its eigenvalue, and inverted as needed so that El Niño events are plotted upward. The correlation coefficient ($r$) between each PC and the Nino3.4 index is given; signficant correlations are marked with an asterisk (autocorrelation-adjusted $p \leq 0.05$, after Bretherton et al. [1999]).

### 3.6. Twentieth Century Trends and Multidecadal Variability

We evaluate long-term salinity trends over the period of 1900–1990, when most coral records are available. This period extends previous studies of global tropical salinity trends by at least 50 years (Boyer et al., 2005; Cheng et al., 2020; Durack & Wijffels, 2010; Helm et al., 2010; Skliris et al., 2014). The coral reconstructions each show freshening of the Pacific ITCZ and SPCZ, with the strongest trends in the western Pacific, and salinification of the southeastern Pacific and Maritime Continent (Figure 8). Both reconstructions also show widespread Atlantic salinification, aside from insignificant freshening trends in the ITCZ region. These trends in the IAP and ORAS5 reconstructions broadly resemble the climatology of SSS (shown by contours in Figure 8), and likely reflect a thermodynamical intensification of the hydrological cycle—that is, a "wet gets wetter, dry gets drier" pattern (Rhein et al., 2013). This pattern is seen in previous salinity studies (albeit over different time periods) and is attributed to increasing atmospheric water vapor transport with temperature (Cheng et al., 2020; Durack et al., 2012; Friedman et al., 2017; Skliris et al., 2014).

The Pacific trends also share many similarities with salinity anomalies observed during El Niño events (e.g., freshening western Pacific and salinifying southeast Pacific; Figure 6 and Figure S10 in Supporting Information S1). These similarities could provide evidence of a long-term weakening in the Walker Circulation (e.g., Power & Kociuba, 2011; Power & Smith, 2007; Vecchi et al., 2006; Zhang & Song, 2006) (contours in Figure S10 of Supporting Information S1). This dynamical response is difficult to disentangle from the thermodynamical component; however, locations that subvert the "fresh gets fresher, salty gets saltier" paradigm can provide evidence of such dynamical changes. The clearest such example is the salinification trend in the climatologically

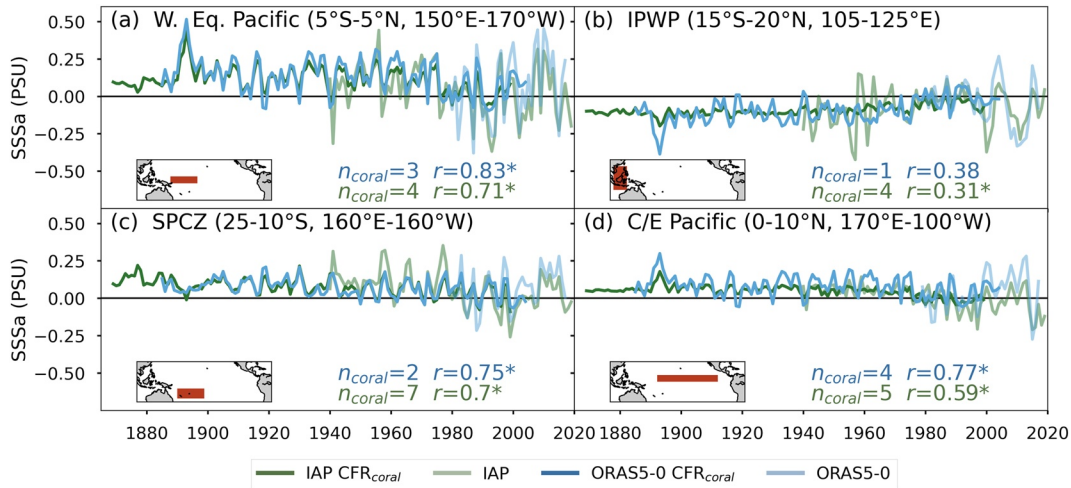


**Figure 7.** Regional mean SSS anomalies (SSSa) for coral CFRs and original SSS data sets (area-weighed; anomalies relative to 1980–1990 reference period). Regions include the western equatorial Pacific (a), a subset of the Indo-Pacific Warm Pool (b), a portion of the South Pacific Convergence Zone (c), and the central/eastern Pacific (d). The number of coral records from each region is given for each reconstruction ($n_{coral}$); the correlation coefficient ($r$) between the coral reconstruction and its respective SSS data set is also given, with significant correlations marked with an asterisk (autocorrelation-adjusted $p \leq 0.05$, after Bretherton et al. [1999]).

fresh Maritime Continent, especially near Borneo, which resembles salinity anomalies in this region during El Niño events (Figure 6). Though this trend may be poorly constrained in our CFRs due to the lack of coral records in this region (Figures 2 and 7b), previous studies nonetheless show similar salinification trends in the Maritime Continent (Cheng et al., 2020; Skliris et al., 2014). This salinification is consistent with decreasing precipitation in this region associated with a weakening of the Pacific Walker circulation. Such weakening is shown in many climate models forced by anthropogenic warming, though observations show strengthening trends in recent decades due to internal variability and/or sulfate aerosol forcing (Bonfils et al., 2020; Chung et al., 2019; England

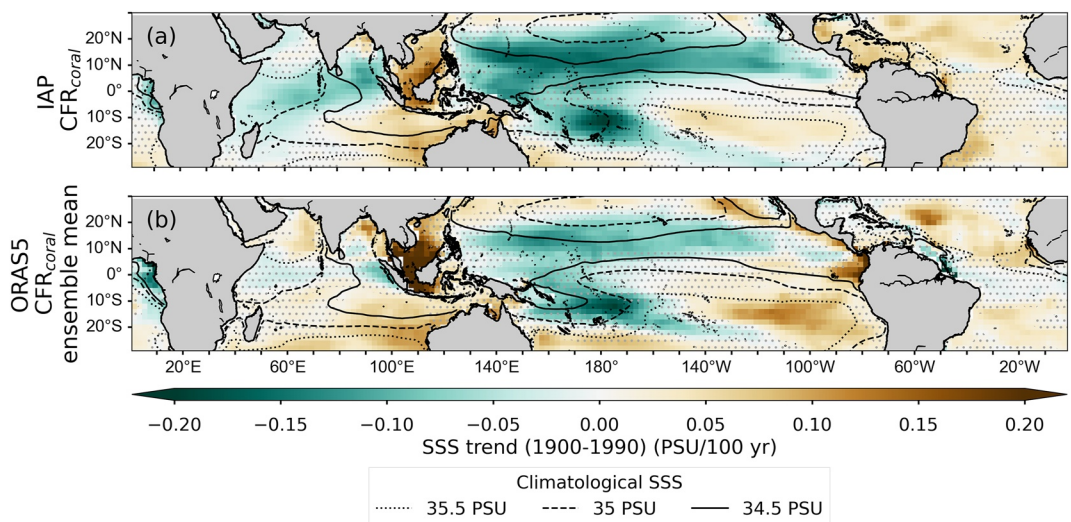


**Figure 8.** Sea surface salinity (SSS) trends (1900–1990) for selected coral-based climate field reconstructions ($CFR_{coral}$), including Institute of Atmospheric Physics (a) and the Ocean ReAnalysis System 5 ensemble mean (b). Trends are computed using OLS regression. Stippling denotes sites where the trend is not significant ($p > 0.05$, calculated from a two-tailed Student's $t$ test with autocorrelation-adjusted sample sizes, see Santer et al. [2000]). Black lines show selected contours (34.5–35.5 PSU) of climatological mean instrumental SSS.

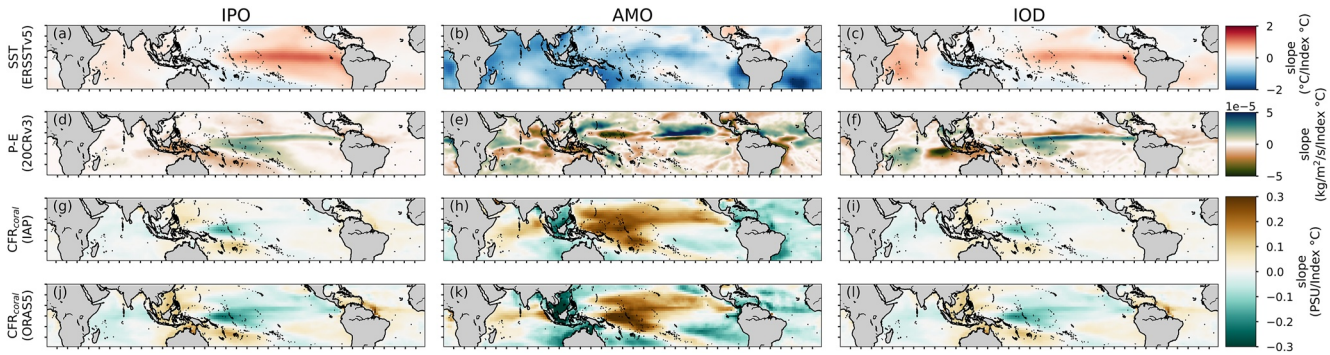


**Figure 9.** Regression slope maps of ERSSTv5-based climate indices, including the Interdecadal Pacific Oscillation (left column), Atlantic Multidecadal Oscillation (center column), and IOD (right column) with sea surface temperature (SST), precipitation minus evaporation (P–E), and the coral-based CFR (CFR$_{coral}$). SST is observation-based (ERSST version 5, Huang et al. [2017]) (a–c); P–E is reanalysis-based (NOAA/CIRES/DOE 20th Century Reanalysis version 3, Slivinski et al. [2021]) (d–f). Coral-based CFRs are based on Institute of Atmospheric Physics (g–i) and the mean across Ocean ReAnalysis System 5 ensemble members (j–l).

et al., 2014; L'Heureux et al., 2013; Plesca et al., 2018; Takahashi & Watanabe, 2016). Ultimately, our coral reconstructions show evidence of multiple potential mechanisms of long-term salinity change.

Freshening trends are also observed in individual salinity-sensitive coral reconstructions in the central Pacific (Nurhati et al., 2011; Sanchez et al., 2020) and SPCZ region (Dassié et al., 2018); indeed, several of these records are used in both the ORAS5 and IAP reconstructions in this study. Freshening trends in individual records from the southern Indonesian Throughflow region (Murty et al., 2018) disagree with insignificant salinification trends in our coral CFRs in the same region (Figure 8). However, those records do not pass the calibration screening criteria for inclusion in the IAP and ORAS5 reconstructions (Figure S2 in Supporting Information S1), so it is possible that these corals are sensitive to fine-scale SSS variability that is not well captured by 1° gridded SSS data sets. We also caution that the region of the Maritime Continent with the largest reconstructed salinification trends (e.g., near Borneo) does not contain any coral $\delta^{18}O$ records with coverage of the early to-mid 20th century, though coral records during the satellite era show a robust salinity signal (Krawczyk et al., 2020); this region would therefore be a suitable target for future coral paleo-salinity work.

In the Indian Ocean, however, salinity trends are less consistent. Both IAP and ORAS5 show salinification in the southeastern Indian Ocean (Figure 8). This salinification may be consistent with a trend toward a positive IOD-like mean state (Abram, Hargreaves, et al., 2020), with decreased P−E in this region during positive IOD events (Figure 9). However, trends are inconsistent in the northern and western Indian Ocean, showing either freshening (IAP) or no significant trends (ORAS5). The Indian Ocean is a noted region of disagreement among salinity studies, and has been attributed to poor observational coverage (Durack & Wijffels, 2010; Skliris et al., 2014). Few salinity-sensitive coral records are available in this region, which could further contribute to these discrepancies in the western and northern Indian Ocean.

Salinity reconstructions also show responses to decadal-and-longer climate variability, though we caution that multidecadal variability may not be well resolved by the 2–4 leading SSS modes that are explicitly reconstructed. During positive Interdecadal Pacific Oscillation (IPO) phases, when eastern and central equatorial Pacific SSTs are anomalously warm, we observe a salinity pattern that generally resembles the response to El Niño events, with freshening in the western equatorial Pacific and much of the Indian Ocean, and salinification in the Maritime Continent and tropical Atlantic (Figure 9, left column, Figure 6). These patterns closely correspond to those shown by reanalysis estimates of P-E over the same time span (Figure 9d). For IAP and ORAS5, the positive AMO phase (i.e., warm north Atlantic) is associated with Atlantic, eastern Pacific, and eastern Indian freshening, and central/western Pacific and western Indian salinification (Figure 9, center column). The similarity between the AMO and IPO SSS patterns highlight the dynamic linkages between these two modes (Meehl et al., 2021). Because these IPO and AMO spatial SSS patterns are similar to observed 20th century trends (though inverted for the AMO) (Figure 8), decadal-to-multidecadal internal variability could complicate the detection of anthropogenic salinity trends over these time scales, as noted in other studies (Gu & Adler, 2013; Stott et al., 2008; N. T. Vinogradova & Ponte, 2017).

## 4. Conclusions

This study demonstrates the utility of coral $\delta^{18}O$ in the spatiotemporal reconstruction of tropical SSS over the full 20th century. Our reconstructions extend existing records of pan-tropical salinity trends by over 50 years (Cheng et al., 2020; Durack et al., 2012; Skliris et al., 2014). These coral-based salinity reconstructions show trends over the 20th century that we attribute to an intensifying hydrological cycle and possibly a weakening Walker Circulation, both superimposed on decadal-to-multidecadal variability.

We identify some key limitations of this reduced-space climate reconstruction approach. Chief among these is a lack of consensus among data sets on the leading modes of salinity variability. Ultimately, the skill of a CFR depends on the accuracy of the salinity data used to generate it. Inconsistencies in the leading modes of variability among SSS reanalyzes—even though these data sets assimilate identical or similar observations—indicate that more work is needed in this regard.

From a coral proxy perspective, there is a pressing need for a gridded surface salinity data set that assimilates all available quality-controlled near-surface observations, is regularly updated to ensure the longest time series possible, and includes uncertainty estimates for calibration with coral data. In the absence of a "gold standard" salinity data set, our results highlight the critical need to compare multiple SSS data sets when examining spatiotemporal variability. Our EOF results demonstrate that IAP and ORAS5 have the most physically plausible salinity variability of the data sets considered in this study. We caution that these results do not necessarily make these data sets more "accurate" than others (a rigorous comparison to observed EN4 profiles would be needed). Nevertheless, the availability of $1\sigma$ uncertainties for IAP make it especially well suited for coral $\delta^{18}O$-SSS calibrations. Therefore, of the data sets considered in this study, IAP meets the most criteria for coral proxy applications.

A second avenue of improvement for this coral-based reconstruction method is the disentanglement of the SST and SSS contributions to coral $\delta^{18}O$. Work is needed (e.g., the PAGES CoralHydro2k project) to improve the $\delta^{18}O_{sw}$ reconstruction methods and expand the network of coral-based $\delta^{18}O_{sw}$ records. Such records could ultimately reconcile discrepancies in trends in regions with suboptimal data availability (e.g., the Indian Ocean and the Maritime Continent).

Despite these limitations, this reduced-space field reconstruction method offers several opportunities to deepen our understanding of both coral $\delta^{18}O$ proxies and tropical Pacific climate variability. This method can be used as a framework to target potential coral sites that can best improve salinity reconstructions and/or extend the reconstruction further into the 19th century, and can be used to develop hypotheses about salinity variability that can be tested against new coral records. For example, western equatorial Pacific sites show high signal-to-noise ratios for reconstructing salinity (Balmaseda et al., 2015); longer paleoclimate records in this region could help constrain interannual to multidecadal salinity variability before the Industrial Era. Finally, this reconstruction method can facilitate proxy-model comparisons. Ultimately, by extending our observational records of tropical oceanic hydroclimate, this climate reconstruction approach can help to disentangle natural variability from anthropogenic trends in a sparsely observed, but climatically crucial, region of the world.

## Data Availability Statement

The Python code for CFR, and the resulting coral-based field reconstructions, are publicly available via Zenodo (Reed et al., 2022).

**Acknowledgments**
This work was supported by National Science Foundation grants OCE-1931242 and OCE-1945479 to DMT, AGS-1501834 to KJA, and a Graduate Research Fellowship to EVR. Additional comments provided by Marcus Lofverstrom, Kaustubh Thirumalai, and Jessica Tierney greatly improved this manuscript.

## References

Abram, N. J., Gagan, M. K., Cole, J. E., Hantoro, W. S., & Mudelsee, M. (2008). Recent intensification of tropical climate variability in the Indian Ocean. *Nature Geoscience*, *1*(12), 849–853. https://doi.org/10.1038/ngeo357

Abram, N. J., Gagan, M. K., McCulloch, M., Chappell, J., & Hantoro, W. (2003). Coral reef death during the 1997 Indian Ocean Dipole linked to Indonesian wildfires. *Science*, *301*(5635), 952–956. https://doi.org/10.1126/science.1091983

Abram, N. J., Hargreaves, J. A., Wright, N. M., Thirumalai, K., Ummenhofer, C. C., & England, M. H. (2020). Palaeoclimate perspectives on the Indian Ocean Dipole. *Quaternary Science Reviews*, *237*, 106302. https://doi.org/10.1016/j.quascirev.2020.106302

Abram, N. J., Wright, N. M., Ellis, B., Dixon, B. C., Wurtzel, J. B., England, M. H., et al. (2020). Coupling of Indo-Pacific climate variability over the last millennium. *Nature*, *579*(7799), 385–392. https://doi.org/10.1038/s41586-020-2084-4

Argo. (2020). Argo float data and metadata from global data assembly Centre [Data set]. Argo GDAC. https://doi.org/10.17882/42182

Balmaseda, M. A., Hernandez, F., Storto, A., Palmer, M. D., Alves, O., Shi, L., et al. (2015). The ocean reanalyses intercomparison project (ORA-IP). *Journal of Operational Oceanography*, *8*(sup1), s80–s97. https://doi.org/10.1080/1755876X.2015.1022329

Behringer, D., & Xue, Y. (2004). Evaluation of the global ocean data assimilation system at NCEP: The Pacific Ocean. In *Eighth symposium on integrated observing and assimilation systems for atmosphere, oceans, and land surface, AMS 84th annual meeting*.

Bingham, F. M., Howden, S. D., & Koblinsky, C. J. (2002). Sea surface salinity measurements in the historical database. *Journal of Geophysical Research*, *107*(12), 1–10. https://doi.org/10.1029/2000jc000767

Bonfils, C. J., Santer, B. D., Fyfe, J. C., Marvel, K., Phillips, T. J., & Zimmerman, S. R. (2020). Human influence on joint changes in temperature, rainfall and continental aridity. *Nature Climate Change*, *10*(8), 726–731. https://doi.org/10.1038/s41558-020-0821-1

Boyer, T. P., Antonov, J. I., Baranova, O. K., Garcia, H. E., Johnson, D. R., Mishonov, A. V., et al. (2013). *World ocean database 2013*. National Oceanographic Data Center (U.S.), Ocean Climate Laboratory. https://doi.org/10.7289/V5NZ85MT

Boyer, T. P., Baranova, O. K., Coleman, C., Garcia, H. E., Grodsky, A., Locarnini, R. A., et al. (2018). *World ocean database 2018* (Technical Report). *NOAA Atlas NESDIS 87*.

Boyer, T. P., Levitus, S., Antonov, J. I., Locarnini, R. A., & Garcia, H. E. (2005). Linear trends in salinity for the World Ocean, 1955–1998. *Geophysical Research Letters*, *32*(1), 1–4. https://doi.org/10.1029/2004GL021791

Bretherton, C. S., Widmann, M., Dymnikov, V. P., Wallace, J. M., & Blade, I. (1999). The effective number of spatial degrees of freedom of a time-varying field. *Journal of Climate*, *12*(7), 1990–2009. https://doi.org/10.1175/1520-0442(1999)012<1990:tenosd>2.0.co;2

Cahyarini, S. Y., Pfeiffer, M., Timm, O., Dullo, W.-C., & Schonberg, D. G. (2008). Reconstructing seawater $\delta^{18}O$ from paired coral $\delta^{18}O$ and Sr/Ca ratios: Methods, error analysis and problems, with examples from Tahiti (French Polynesia) and Timor (Indonesia). *Geochimica et Cosmochimica Acta*, *72*(12), 2841–2853. https://doi.org/10.1016/j.gca.2008.04.005

Carton, J. A., Chepurin, G. A., & Chen, L. (2018). SODA3: A new ocean climate reanalysis. *Journal of Climate*, *31*(17), 6967–6983. https://doi.org/10.1175/jcli-d-18-0149.1

Carton, J. A., Chepurin, G. A., Chen, L., & Grodsky, S. A. (2018). Improved global net surface heat flux. *Journal of Geophysical Research: Oceans*, *123*(5), 3144–3163. https://doi.org/10.1002/2017JC013137

Carton, J. A., & Giese, B. S. (2008). A reanalysis of ocean climate using Simple Ocean Data Assimilation (SODA). *Monthly Weather Review*, *136*(8), 2999–3017. https://doi.org/10.1175/2007MWR1978.1

Cheng, L., Trenberth, K. E., Gruber, N., Abraham, J. P., Fasullo, J. T., Li, G., et al. (2020). Improved estimates of changes in upper ocean salinity and the hydrological cycle. *Journal of Climate*, *33*(23), 10357–10381. https://doi.org/10.1175/JCLI-D-20-0366.1

Cheng, L., & Zhu, J. (2014). Artifacts in variations of ocean heat content induced by the observation system changes. *Geophysical Research Letters*, *41*, 7276–7283. https://doi.org/10.1002/2014GL061881

Chi, J., Qu, T., Du, Y., Qi, J., & Shi, P. (2022). Ocean salinity indices of interannual modes in the tropical Pacific. *Climate Dynamics*, *58*(1–2), 369–387. https://doi.org/10.1007/s00382-021-05911-9

Chung, E. S., Timmermann, A., Soden, B. J., Ha, K. J., Shi, L., & John, V. O. (2019). Reconciling opposing Walker circulation trends in observations and model projections. *Nature Climate Change*, *9*(5), 405–412. https://doi.org/10.1038/s41558-019-0446-4

Cobb, K. M., Charles, C. D., Cheng, H., & Edwards, R. L. (2003). El Niño/Southern Oscillation and tropical Pacific climate during the last millennium. *Nature*, *424*(6946), 271–276. https://doi.org/10.1038/nature01779

Cobb, K. M., Westphal, N., Sayani, H. R., Watson, J. T., Di Lorenzo, E., Cheng, H., et al. (2013). Highly variable El Niño-Southern Oscillation throughout the Holocene. *Science*, *339*(6115), 67–70. https://doi.org/10.1126/science.1228246

Cole, J. E., & Fairbanks, R. G. (1990). The Southern Oscillation recorded in the $\delta^{18}O$ of corals from Tarawa Atoll. *Paleoceanography*, *5*(5), 669–683. https://doi.org/10.1029/PA005i005p00669

Conroy, J., Thompson, D., Cobb, K., Noone, D., Rea, S., & Legrande, A. (2017). Spatiotemporal variability in the $\delta^{18}O$-salinity relationship of seawater across the tropical Pacific Ocean. *Paleoceanography*, *32*(5), 484–497. https://doi.org/10.1002/2016PA003073

Cook, B. I., Cook, E. R., Anchukaitis, K. J., Seager, R., & Miller, R. L. (2011). Forced and unforced variability of twentieth century North American droughts and pluvials. *Climate Dynamics*, *37*(5), 1097–1110. https://doi.org/10.1007/s00382-010-0897-9

Dassié, E. P., Hasson, A., Khodri, M., Lebas, N., & Linsley, B. K. (2018). Spatiotemporal variability of the South Pacific Convergence Zone fresh pool eastern front from coral-derived surface salinity data. *Journal of Climate*, *31*(8), 3265–3288. https://doi.org/10.1175/JCLI-D-17-0071.1

Delcroix, T., Alory, G., Cravatte, S., Corrège, T., & McPhaden, M. J. (2011). A gridded sea surface salinity data set for the tropical Pacific with sample applications (1950–2008). *Deep-Sea Research Part I: Oceanographic Research Papers*, *58*(1), 38–48. https://doi.org/10.1016/j.dsr.2010.11.002

Durack, P. J., & Wijffels, S. E. (2010). Fifty-year trends in global ocean salinities and their relationship to broad-scale warming. *Journal of Climate*, *23*(16), 4342–4362. https://doi.org/10.1175/2010JCLI3377.1

Durack, P. J., Wijffels, S. E., & Matear, R. J. (2012). Ocean salinities reveal strong global water cycle intensification during 1950 to 2000. *Science*, *336*(6080), 455–458. https://doi.org/10.1126/science.1212222

Emile-Geay, J., Cobb, K. M., Mann, M. E., & Wittenberg, A. T. (2013a). Estimating central equatorial Pacific SST variability over the past millennium. Part I: Methodology and validation. *Journal of Climate*, *26*(7), 2302–2328. https://doi.org/10.1175/JCLI-D-11-00510.1

Emile-Geay, J., Cobb, K. M., Mann, M. E., & Wittenberg, A. T. (2013b). Estimating central equatorial Pacific SST variability over the past millennium. Part II: Reconstructions and implications. *Journal of Climate*, *26*(7), 2329–2352. https://doi.org/10.1175/JCLI-D-11-00511.1

England, M. H., Mcgregor, S., Spence, P., Meehl, G. A., Timmermann, A., Cai, W., et al. (2014). Recent intensification of wind-driven circulation in the Pacific and the ongoing warming hiatus. *Nature Climate Change*, *4*(3), 222–227. https://doi.org/10.1038/nclimate2106

Evans, M. N., Kaplan, A., & Cane, M. A. (2000). Intercomparison of coral oxygen isotope data and historical sea surface temperature (SST): Potential for coral-based SST field reconstructions. *Paleoceanography*, *15*(5), 551–563. https://doi.org/10.1029/2000PA000498

Evans, M. N., Kaplan, A., & Cane, M. A. (2002). Pacific sea surface temperature field reconstruction from coral $\delta^{18}O$ data using reduced space objective analysis. *Paleoceanography*, *17*(1), 7-1–7-13. https://doi.org/10.1029/2000pa000590

Fairbanks, R. G., Evans, M. N., Rubenstone, J. L., Mortlock, R. A., Broad, K., Moore, M. D., & Charles, C. D. (1997). Evaluating climate indices and their geochemical proxies measured in corals. *Coral Reefs*, *16*(SUPPL. 1), 93–100. https://doi.org/10.1007/s003380050245

Friedman, A. R., Reverdin, G., Khodri, M., & Gastineau, G. (2017). A new record of Atlantic sea surface salinity from 1896 to 2013 reveals the signatures of climate variability and long-term trends. *Geophysical Research Letters*, *44*(4), 1866–1876. https://doi.org/10.1002/2017GL072582

Fritts, H., Blasing, T., Hayden, B., & Kutzback, J. (1971). Multivariate techniques for specifying tree-growth and climate relationships and for reconstructing anomalies in paleoclimate. *Journal of Applied Meteorology*, *10*(5), 845–864. https://doi.org/10.1175/1520-0450(1971)010<0845:mtfstg>2.0.co;2

Giese, B. S., & Ray, S. (2011). El Niño variability in simple ocean data assimilation (SODA), 1871–2008. *Journal of Geophysical Research*, *116*(2), 1–17. https://doi.org/10.1029/2010JC006695

Gill, E. C., Rajagopalan, B., Molnar, P., & Marchitto, T. M. (2016). Reduced-dimension reconstruction of the equatorial Pacific SST and zonal wind fields over the past 10,000 years using Mg/Ca and alkenone records. *Paleoceanography*, *31*(7), 928–952. https://doi.org/10.1002/2016PA002948

Good, S. A., Martin, M. J., & Rayner, N. A. (2013). EN4: Quality controlled ocean temperature and salinity profiles and monthly objective analyses with uncertainty estimates. *Journal of Geophysical Research: Oceans*, *118*(12), 6704–6716. https://doi.org/10.1002/2013JC009067

Gorman, M. K., Quinn, T. M., Taylor, F. W., Partin, J. W., Cabioch, G., Austin, J. A., et al. (2012). A coral-based reconstruction of sea surface salinity at Sabine Bank, Vanuatu from 1842 to 2007 CE. *Paleoceanography*, *27*(3), 1–13. https://doi.org/10.1029/2012PA002302

Gouretski, V., & Reseghetti, F. (2010). On depth and temperature biases in bathythermograph data: Development of a new correction scheme based on analysis of a global ocean database. *Deep Sea Research Part I: Oceanographic Research Papers*, *57*(6), 812–833. https://doi.org/10.1016/j.dsr.2010.03.011

Green, B., Marshall, J., Green, B., & Marshall, J. (2017). Coupling of trade winds with ocean circulation damps ITCZ shifts. *Journal of Climate*, *30*(12), 4395–4411. https://doi.org/10.1175/JCLI-D-16-0818.1

Grothe, P. R., Cobb, K. M., Liguori, G., Di Lorenzo, E., Capotondi, A., Lu, Y., et al. (2020). Enhanced El Niño–Southern Oscillation variability in recent decades. *Geophysical Research Letters*, *47*(7). https://doi.org/10.1029/2019GL083906

Gu, G., & Adler, R. F. (2013). Interdecadal variability/long-term changes in global precipitation patterns during the past three decades: Global warming and/or Pacific decadal variability? *Climate Dynamics*, *40*(11–12), 3009–3022. https://doi.org/10.1007/s00382-012-1443-8

Harris, C. R., Millman, K. J., van der Walt, S. J., Gommers, R., Virtanen, P., Cournapeau, D., et al. (2020). Array programming with NumPy. *Nature*, *585*(7825), 357–362. https://doi.org/10.1038/s41586-020-2649-2

Helm, K. P., Bindoff, N. L., & Church, J. A. (2010). Changes in the global hydrological-cycle inferred from ocean salinity. *Geophysical Research Letters*, *37*(18), 2–6. https://doi.org/10.1029/2010GL044222

Hendy, E. J., Gagan, M. K., Alibert, C. A., McCulloch, M. T., Lough, J. M., & Isdale, P. J. (2002). Abrupt decrease in tropical Pacific sea surface salinity at end of Little Ice Age. *Science*, *295*(5559), 1511–1514. https://doi.org/10.1126/science.1067693

Henley, B. J., Gergis, J., Karoly, D. J., Power, S., Kennedy, J., & Folland, C. K. (2015). A Tripole Index for the Interdecadal Pacific Oscillation. *Climate Dynamics*, *45*(11–12), 3077–3090. https://doi.org/10.1007/s00382-015-2525-1

Huang, B., Thorne, P. W., Banzon, V. F., Boyer, T., Chepurin, G., Lawrimore, J. H., et al. (2017). Extended reconstructed sea surface temperature, version 5 (ERSSTv5): Upgrades, validations, and intercomparisons. *Journal of Climate*, *30*(20), 8179–8205. https://doi.org/10.1175/jcli-d-16-0836.1

Huang, B., Xue, Y., & Behringer, D. W. (2008). Impacts of Argo salinity in NCEP global ocean data assimilation system: The tropical Indian Ocean. *Journal of Geophysical Research*, *113*(8), C08002. https://doi.org/10.1029/2007JC004388

IOC, SCOR, & IAPSO. (2010). The International thermodynamic equation of seawater - 2010: Calculation and use of thermodynamic properties. In *Intergovernmental Oceanographic Commission, Manuals and Guides* (Vol. 56, p. 196). UNESCO.

Kilbourne, K. H., Quinn, T. M., Taylor, F. W., Delcroix, T., & Gouriou, Y. (2004). El Niño-Southern Oscillation-related salinity variations recorded in the skeletal geochemistry of a Porites coral from Espiritu Santo, Vanuatu. *Paleoceanography*, *19*(4). https://doi.org/10.1029/2004PA001033

Konecky, B. L., McKay, N. P., Churakova, O. V., Comas-Bru, L., Dassié, E. P., DeLong, K. L., et al. (2020). The Iso2k database: A global compilation of paleo-$\delta^{18}O$ and $\delta^{2}H$ records to aid understanding of common era climate. *Earth System Science Data*, *12*(3), 2261–2288. https://doi.org/10.5194/essd-12-2261-2020

Krawczyk, H., Zinke, J., Browne, N., Struck, U., McIlwain, J., O'Leary, M., & Garbe-Schönberg, D. (2020). Corals reveal ENSO-driven synchrony of climate impacts on both terrestrial and marine ecosystems in northern Borneo. *Scientific Reports*, *10*(1), 1–14. https://doi.org/10.1038/s41598-020-60525-1

LeGrande, A. N., & Schmidt, G. A. (2006). Global gridded data set of the oxygen isotopic composition in seawater. *Geophysical Research Letters*, *33*(12), 1–5. https://doi.org/10.1029/2006GL026011

Legrande, A. N., & Schmidt, G. A. (2011). Water isotopologues as a quantitative paleosalinity proxy. *Paleoceanography*, *26*(3), 1–10. https://doi.org/10.1029/2010PA002043

L'Heureux, M. L., Lee, S., & Lyon, B. (2013). Recent multidecadal strengthening of the Walker circulation across the tropical Pacific. *Nature Climate Change*, *3*(6), 571–576. https://doi.org/10.1038/nclimate1840

Linsley, B. K., Dunbar, R. B., Lee, D., Tangri, N., & Dassié, E. (2017). Abrupt northward shift of SPCZ position in the late-1920s indicates coordinated Atlantic and Pacific ITCZ change. *Past Global Changes Magazine*, *25*(1), 52–56. https://doi.org/10.22498/pages.25.1.52

Linsley, B. K., Kaplan, A., Gouriou, Y., Salinger, J., DeMenocal, P. B., Wellington, G. M., & Howe, S. S. (2006). Tracking the extent of the South Pacific Convergence Zone since the early 1600s. *Geochemistry, Geophysics, Geosystems*, *7*(5), 1–15. https://doi.org/10.1029/2005GC001115

Linsley, B. K., Wellington, G. M., Schrag, D. P., Ren, L., Salinger, M. J., & Tudhope, A. W. (2004). Geochemical evidence from corals for changes in the amplitude and spatial pattern of South Pacific interdecadal climate variability over the last 300 years. *Climate Dynamics*, *22*(1), 1–11. https://doi.org/10.1007/s00382-003-0364-y

Linsley, B. K., Wu, H. C., Dassié, E. P., & Schrag, D. P. (2015). Decadal changes in South Pacific sea surface temperatures and the relationship to the Pacific decadal oscillation and upper ocean heat content. *Geophysical Research Letters*, *42*(7), 2358–2366. https://doi.org/10.1002/2015GL063045.Received

Mann, M. E., Bradley, R. S., & Hughes, M. K. (1998). Global-scale temperature patterns and climate forcing over the past six centuries. *Nature*, *392*(6678), 779–787. https://doi.org/10.1038/33859

McConnaughey, T. (1989). $^{13}C$ and $^{18}O$ isotopic disequilibrium in biological carbonates: I. Patterns. *Geochimica et Cosmochimica Acta*, *53*(1), 151–162. https://doi.org/10.1016/0016-7037(89)90282-2

Meehl, G. A., Hu, A., Castruccio, F., England, M. H., Bates, S. C., Danabasoglu, G., et al. (2021). Atlantic and Pacific tropics connected by mutually interactive decadal-timescale processes. *Nature Geoscience*, *14*(1), 36–42. https://doi.org/10.1038/s41561-020-00669-x

Miles, J. (2014). *R squared, adjusted R squared*. In *Wiley StatsRef: Statistics Reference Online* (Vol. 2, pp. 2–4). https://doi.org/10.1002/9781118445112.stat06627

Murty, S. A., Goodkin, N. F., Wiguna, A. A., & Gordon, A. L. (2018). Variability in coral-reconstructed sea surface salinity between the northern and southern Lombok Strait linked to East Asian winter monsoon mean state reversals. *Paleoceanography and Paleoclimatology*, *33*(10), 1116–1133. https://doi.org/10.1029/2018PA003387

Nurhati, I. S., Cobb, K. M., & Di Lorenzo, E. (2011). Decadal-scale SST and salinity variations in the central tropical Pacific: Signatures of natural and anthropogenic climate change. *Journal of Climate*, *24*(13), 3294–3308. https://doi.org/10.1175/2011JCLI3852.1

Plesca, E., Grützun, V., & Buehler, S. A. (2018). How robust is the weakening of the Pacific Walker circulation in CMIP5 idealized transient climate simulations? *Journal of Climate*, *31*(1), 81–97. https://doi.org/10.1175/JCLI-D-17-0151.1

Power, S. B., & Kociuba, G. (2011). What caused the observed twentieth-century weakening of the Walker Circulation? *Journal of Climate*, *24*(24), 6501–6514. https://doi.org/10.1175/2011JCLI4101.1

Power, S. B., & Smith, I. N. (2007). Weakening of the Walker Circulation and apparent dominance of El Niño both reach record levels, but has ENSO really changed? *Geophysical Research Letters*, *34*(18), 2–5. https://doi.org/10.1029/2007GL030854

Qi, J., Zhang, L., Qu, T., Yin, B., Xu, Z., Yang, D., et al. (2019). Salinity variability in the tropical Pacific during the central-Pacific and eastern-Pacific El Niño events. *Journal of Marine Systems*, *199*, 103225. https://doi.org/10.1016/j.jmarsys.2019.103225

Reed, E., Thompson, D., & Anchukaitis, K. (2022). Coral-based sea surface salinity reconstructions and the role of observational uncertainties in inferred variability and trends: Original release (version 1.0.0) [Open access software] [Data set]. Zenodo. https://doi.org/10.5281/zenodo.6403156

Ren, L., Linsley, B. K., Wellington, G. M., Schrag, D. P., & Hoegh-Guldberg, O. (2002). Deconvolving the $\delta^{18}O$ seawater component from subseasonal coral $\delta^{18}O$ and Sr/Ca at Rarotonga in the southwestern subtropical Pacific for the period 1726 to 1997. *Geochimica et Cosmochimica Acta*, *67*(9), 1609–1621. https://doi.org/10.1016/S0016-7037(02)00917-1

Rhein, M., Rintoul, S., Aoki, S., Campos, E., Chambers, D., Feely, R., et al. (2013). Observations: Ocean. In T. Stocker, G.-K. Qin, M. Plattner, S. K. Tignor, J. Allen, A. Boschung, et al. (Eds.), *Climate change 2013: The physical science basis. Contribution of Working Group I to the Fifth Assessment Report of the Intergovernmental Panel on Climate Change*. Cambridge University Press. https://doi.org/10.1007/s11802-014-2206-4

Russon, T., Tudhope, A. W., Hegerl, G. C., Collins, M., & Tindall, J. (2013). Inter-annual tropical Pacific climate variability in an isotope-enabled CGCM: Implications for interpreting coral stable oxygen isotope records of ENSO. *Climate of the Past*, *9*(4), 1543–1557. https://doi.org/10.5194/cp-9-1543-2013

Saha, S., Nadiga, S., Thiaw, C., Wang, J., Wang, W., Zhang, Q., et al. (2006). The NCEP climate forecast system. *Journal of Climate*, *19*(15), 3483–3517. https://doi.org/10.1175/JCLI3812.1

Saji, N. H., Goswami, B. N., Vinayachandran, P. N., & Yamagata, T. (1999). A dipole mode in the tropical Indian Ocean. *Nature*, *401*(6751), 360–364. https://doi.org/10.1038/43854

Sanchez, S. C., Hakim, G. J., & Saenger, C. P. (2021). Climate model teleconnection patterns govern the Niño-3.4 response to early nineteenth-century volcanism in coral-based data assimilation reconstructions. *Journal of Climate*, *34*(5), 1863–1880. https://doi.org/10.1175/JCLI-D-20-0549.1

Sanchez, S. C., Westphal, N., Haug, G. H., Cheng, H., Edwards, R. L., Schneider, T., et al. (2020). A continuous record of central tropical Pacific climate since the midnineteenth century reconstructed from Fanning and Palmyra Island corals: A case study in coral data reanalysis. *Paleoceanography and Paleoclimatology*, *35*(8), 1–15. https://doi.org/10.1029/2020PA003848

Santer, B. D., Wigley, T. M., Boyle, J. S., Gaffen, D. J., Hnilo, J. J., Nychka, D., et al. (2000). Statistical significance of trends and trend differences in layer-average atmospheric temperature time series. *Journal of Geophysical Research*, *105*(D6), 7337–7356. https://doi.org/10.1029/1999JD901105

Schneider, U., Finger, P., Meyer-Christoffer, A., Rustemeier, E., Ziese, M., & Becker, A. (2017). Evaluating the hydrological cycle over land using the newly-corrected precipitation climatology from the Global Precipitation Climatology Centre (GPCC). *Atmosphere*, *8*(3), 52. https://doi.org/10.3390/atmos8030052

Singh, A., Delcroix, T., & Cravatte, S. (2011). Contrasting the flavors of El Niño-Southern Oscillation using sea surface salinity observations. *Journal of Geophysical Research*, *116*(6), 1–16. https://doi.org/10.1029/2010JC006862

Skliris, N., Marsh, R., Josey, S. A., Good, S. A., Liu, C., & Allan, R. P. (2014). Salinity changes in the World Ocean since 1950 in relation to changing surface freshwater fluxes. *Climate Dynamics*, *43*(3–4), 709–736. https://doi.org/10.1007/s00382-014-2131-7

Slivinski, L. C., Compo, G. P., Sardeshmukh, P. D., Whitaker, J. S., McColl, C., Allan, R. J., et al. (2021). An evaluation of the performance of the twentieth century reanalysis version 3. *Journal of Climate*, *34*(4), 1417–1438. https://doi.org/10.1175/JCLI-D-20-0505.1

Smith, T. M., Arkin, P. A., Ren, L., & Shen, S. S. (2012). Improved reconstruction of global precipitation since 1900. *Journal of Atmospheric and Oceanic Technology*, *29*(10), 1505–1517. https://doi.org/10.1175/JTECH-D-12-00001.1

Stevenson, S., Overpeck, J. T., Fasullo, J., Coats, S., Parsons, L., Otto-Bliesner, B., et al. (2018). Climate variability, volcanic forcing, and last millennium hydroclimate extremes. *Journal of Climate*, *31*(11), 4309–4327. https://doi.org/10.1175/JCLI-D-17-0407.1

Storto, A., Alvera-Azcárate, A., Balmaseda, M. A., Barth, A., Chevallier, M., Counillon, F., et al. (2019). Ocean reanalyses: Recent advances and unsolved challenges. *Frontiers in Marine Science*, *6*, 1–10. https://doi.org/10.3389/fmars.2019.00418

Stott, P. A., Sutton, R. T., & Smith, D. M. (2008). Detection and attribution of Atlantic salinity changes. *Geophysical Research Letters*, *35*(21), 1–5. https://doi.org/10.1029/2008GL035874

Sun, C., Thresher, A., Keeley, R., Hall, N., Hamilton, M., Chinn, P., et al. (2010). The data management system for the global temperature and salinity profile programme. In J. Hall, D. Harrison, & D. Stammer (Eds.), *Proceedings of OceanObs. 09: Sustained Ocean Observations and Information for Society* (pp. 1–15). ESA Publication WPP-306. https://doi.org/10.5270/OceanObs09.cwp.86

Takahashi, C., & Watanabe, M. (2016). Pacific trade winds accelerated by aerosol forcing over the past two decades. *Nature Climate Change*, *6*(8), 768–772. https://doi.org/10.1038/nclimate2996

Terray, L., Corre, L., Cravatte, S., Delcroix, T., Reverdin, G., & Ribes, A. (2012). Near-surface salinity as nature's rain gauge to detect human influence on the tropical water cycle. *Journal of Climate*, *25*(3), 958–977. https://doi.org/10.1175/JCLI-D-10-05025.1

Thirumalai, K., Singh, A., & Ramesh, R. (2011). A MATLAB™ code to perform weighted linear regression with (correlated or uncorrelated) errors in bivariate data. *Journal of the Geological Society of India*, *77*(4), 377–380. https://doi.org/10.1007/s12594-011-0044-1

Thompson, D. M., Ault, T. R., Evans, M. N., Cole, J. E., & Emile-Geay, J. (2011). Comparison of observed and simulated tropical climate trends using a forward model of coral $\delta^{18}O$. *Geophysical Research Letters*, *38*(14), 1–6. https://doi.org/10.1029/2011GL048224

Tierney, J. E., Abram, N. J., Anchukaitis, K. J., Evans, M. N., Giry, C., Kilbourne, K. H., et al. (2015). Tropical sea surface temperatures for the past four centuries reconstructed from coral archives. *Paleoceanography*, *30*(3), 226–252. https://doi.org/10.1002/2014PA002717.Received

Trenberth, K. E., & Shea, D. J. (2006). Atlantic hurricanes and natural variability in 2005. *Geophysical Research Letters*, *33*(12), L12704. https://doi.org/10.1029/2006GL026894

Vecchi, G. A., Soden, B. J., Wittenberg, A. T., Held, I. M., Leetmaa, A., & Harrison, M. J. (2006). Weakening of tropical Pacific atmospheric circulation due to anthropogenic forcing. *Nature*, *441*(1), 73–76. https://doi.org/10.1038/nature04744

Vinogradova, N., Lee, T., Boutin, J., Drushka, K., Fournier, S., Sabia, R., et al. (2019). Satellite salinity observing system: Recent discoveries and the way forward. *Frontiers in Marine Science*, *6*, 1–23. https://doi.org/10.3389/fmars.2019.00243

Vinogradova, N. T., & Ponte, R. M. (2013). Clarifying the link between surface salinity and freshwater fluxes on monthly to interannual time scales. *Journal of Geophysical Research: Oceans*, *118*(6), 3190–3201. https://doi.org/10.1002/jgrc.20200

Vinogradova, N. T., & Ponte, R. M. (2017). In search of fingerprints of the recent intensification of the ocean water cycle. *Journal of Climate*, *30*(14), 5513–5528. https://doi.org/10.1175/JCLI-D-16-0626.1

Virtanen, P., Gommers, R., Oliphant, T. E., Haberland, M., Reddy, T., Cournapeau, D., et al. (2020). SciPy 1.0: Fundamental algorithms for scientific computing in Python. *Nature Methods*, *17*(3), 261–272. https://doi.org/10.1038/s41592-019-0686-2

Wilks, D. (2006). *Statistical methods in the atmospheric sciences*. Academic Press.

Xue, Y., Wen, C., Kumar, A., Balmaseda, M., Fujii, Y., Alves, O., et al. (2017). A real-time ocean reanalyses intercomparison project in the context of tropical Pacific observing system and ENSO monitoring. *Climate Dynamics*, *49*(11–12), 3647–3672. https://doi.org/10.1007/s00382-017-3535-y

Yu, L. (2011). A global relationship between the ocean water cycle and near-surface salinity. *Journal of Geophysical Research*, *116*(10), 1–17. https://doi.org/10.1029/2010JC006937

Zhang, M., & Song, H. (2006). Evidence of deceleration of atmospheric vertical overturning circulation over the tropical Pacific. *Geophysical Research Letters*, *33*(12), 1–5. https://doi.org/10.1029/2006GL025942

Zuo, H., Balmaseda, M. A., de Boisseson, E., Hirahara, S., Chrust, M., & de Rosnay, P. (2017). A generic ensemble generation scheme for data assimilation and ocean analysis. *ECMWF Technical Memoranda*, *795*, 44.

Zuo, H., Balmaseda, M. A., Tietsche, S., Mogensen, K., & Mayer, M. (2019). The ECMWF operational ensemble reanalysis-analysis system for ocean and sea ice: A description of the system and assessment. *Ocean Science*, *15*(3), 779–808. https://doi.org/10.5194/os-15-779-2019

## References From the Supporting Information

Abram, N. J., Dixon, B. C., Rosevear, M. G., Plunkett, B., Gagan, M. K., Hantoro, W. S., & Phipps, S. J. (2015). Optimized coral reconstructions of the Indian Ocean Dipole: An assessment of location and length considerations. *Paleoceanography*, *30*(10), 1391–1405. https://doi.org/10.1002/2015PA002810

Asami, R., Yamada, T., Iryu, Y., Quinn, T. M., Meyer, C. P., & Paulay, G. (2005). Interannual and decadal variability of the western Pacific sea surface condition for the years 1787–2000: Reconstruction based on stable isotope record from a Guam coral. *Journal of Geophysical Research*, *110*(C5), 1–13. https://doi.org/10.1029/2004JC002555

Boiseau, M., Juillet-Leclerc, A., Yiou, P., Salvat, B., Isdale, P., & Guillaume, M. (1998). Atmospheric and oceanic evidences of El Nino-Southern Oscillation events in the south central Pacific Ocean from coral stable isotopic records over the last 137 years. *Paleoceanography*, *13*(6), 671–685. https://doi.org/10.1029/98PA02502

Cahyarini, S. Y., Pfeiffer, M., Nurhati, I. S., Aldrian, E., Dullo, W.-C., & Hetzinger, S. (2014). Twentieth century sea surface temperature and salinity variations at Timor inferred from paired coral $\delta^{18}O$ and Sr/Ca measurements. *Journal of Geophysical Research: Oceans*, *119*(7), 4593–4604. https://doi.org/10.1002/2013JC009594

Calvo, E., Marshall, J. F., Pelejero, C., McCulloch, M. T., Gagan, M. K., & Lough, J. M. (2007). Interdecadal climate variability in the coral sea since 1708 A.D. *Palaeogeography, Palaeoclimatology, Palaeoecology*, *248*(1–2), 190–201. https://doi.org/10.1016/j.palaeo.2006.12.003

Carilli, J. E., Charles, C. D., Garren, M., McField, M., & Norris, R. D. (2013). Baseline shifts in coral skeletal oxygen isotopic composition: A signature of symbiont shuffling? *Coral Reefs*, *32*(2), 559–571. https://doi.org/10.1007/s00338-012-1004-y

Carilli, J. E., McGregor, H. V., Gaudry, J. J., Donner, S. D., Gagan, M. K., Stevenson, S., et al. (2014). Equatorial Pacific coral geochemical records show recent weakening of the Walker Circulation. *Paleoceanography*, *29*(11), 1–15. https://doi.org/10.1002/2014PA002683

Chakraborty, S., & Ramesh, R. (1998). Stable isotope variations in a coral (Favia speciosa) from the Gulf of Kutch during 1948–1989 A.D.: Environmental implications. *Proceedings of the Indian Academy of Sciences - Earth & Planetary Sciences*, *107*(4), 331–341. https://doi.org/10.1007/BF02841599

Charles, C. D., Cobb, K., Moore, M. D., & Fairbanks, R. G. (2003). Monsoon–tropical ocean interaction in a network of coral records spanning the 20th century. *Marine Geology*, *201*(1–3), 207–222. https://doi.org/10.1016/S0025-3227(03)00217-2

Charles, C. D., Hunter, D. E., & Fairbanks, R. G. (1997). Interaction between the ENSO and the Asian monsoon in a coral record of tropical climate. *Science*, *277*(5328), 925–928. https://doi.org/10.1126/science.277.5328.925

Cole, J. E., Dunbar, R. B., McClanahan, T. R., & Muthiga, N. A. (2000). Tropical Pacific forcing of decadal SST variability in the western Indian Ocean over the past two centuries. *Science*, *287*(5453), 617–619. https://doi.org/10.1126/science.287.5453.617

Cole, J. E., Fairbanks, R. G., & Shen, G. T. (1993). Recent variability in the Southern Oscillation: Isotopic results from a Tarawa Atoll coral. *Science*, *260*(5115), 1790–1793. https://doi.org/10.1126/science.260.5115.1790

Cross-Validation. (2010). In C. Sammut & G. I. Webb (Eds.), *Encyclopedia of machine learning* (p. 249). Springer. https://doi.org/10.1007/978-0-387-30164-8_190

Damassa, T. D., Cole, J. E., Barnett, H. R., Ault, T. R., & McClanahan, T. R. (2006). Enhanced multidecadal climate variability in the seventeenth century from coral isotope records in the western Indian Ocean. *Paleoceanography*, *21*(2), 1–15. https://doi.org/10.1029/2005PA001217

Deng, W., Wei, G., Xie, L., & Yu, K. (2013). Environmental controls on coral skeletal $\delta^{13}C$ in the northern South China Sea. *Journal of Geophysical Research: Biogeosciences*, *118*(4), 1359–1368. https://doi.org/10.1002/jgrg.20116

Druffel, E. R., & Griffin, S. (1999). Variability of surface ocean radiocarbon and stable isotopes in the southwestern Pacific. *Journal of Geophysical Research*, *104*(C10), 23607–23613. https://doi.org/10.1029/1999jc900212

Dunbar, R. B., Wellington, G. M., Colgan, M. W., & W, G. P. (1994). Eastern Pacific sea surface temperature since 1600 A.D.: The record of $\delta^{18}O$ climate variability in Galápagos Corals. *Paleobiology*, *9*(2), 291–315. https://doi.org/10.1029/93PA03501

Evans, M., Kaplan, A., Cane, M., & Villalba, R. (2001). Globality and optimality in climate field reconstructions from proxy data. *Interhemispheric climate linkages* (pp. 53–XV). Academic Press. https://doi.org/10.1016/b978-012472670-3/50007-0

Evans, M. N., Fairbanks, R. G., & Rubenstone, J. L. (1998). A proxy index of ENSO teleconnections. *Nature*, *394*(6695), 732–733. https://doi.org/10.1038/29424

Felis, T., Pätzold, J., Loya, Y., Fine, M., Nawar, A. H., & Wefer, G. (2000). A coral oxygen isotope record from the northern Red Sea documenting NAO, ENSO, and North Pacific teleconnections on Middle East climate variability since the year 1750. *Paleoceanography*, *15*(6), 679–694. https://doi.org/10.1029/1999PA000477

Goodkin, N. F., Hughen, K. A., Doney, S. C., & Curry, W. B. (2008). Increased multidecadal variability of the North Atlantic Oscillation since 1781. *Nature Geoscience*, *1*(12), 844–848. https://doi.org/10.1038/ngeo352

Guilderson, T. P., & Schrag, D. P. (1999). Reliability of coral isotope records from the western Pacific warm pool: A comparison using age-optimized records. *Paleoceanography*, *14*(4), 457–464. https://doi.org/10.1029/1999PA900024

Heiss, G. A. (1994). Coral reefs in the Red Sea: Growth, production and stable isotopes. *GEOMAR-Report*, *32*, 1–141.

Hennekam, R., Zinke, J., van Sebille, E., ten Have, M., Brummer, G. J. A., & Reichart, G. J. (2018). Cocos (Keeling) corals reveal 200 years of multidecadal modulation of southeast Indian Ocean hydrology by Indonesian throughflow. *Paleoceanography and Paleoclimatology*, *33*(1), 48–60. https://doi.org/10.1002/2017PA003181

Hetzinger, S., Pfeiffer, M., Dullo, W. C., Garbe-Schönberg, D., & Halfar, J. (2010). Rapid 20th century warming in the Caribbean and impact of remote forcing on climate in the northern tropical Atlantic as recorded in a Guadeloupe coral. *Palaeogeography, Palaeoclimatology, Palaeoecology*, *296*(1–2), 111–124. https://doi.org/10.1016/j.palaeo.2010.06.019

Hetzinger, S., Pfeiffer, M., Dullo, W. C., Keenlyside, N., Latif, M., & Zinke, J. (2008). Caribbean coral tracks Atlantic Multidecadal Oscillation and past hurricane activity. *Geology*, *36*(1), 11–14. https://doi.org/10.1130/G24321A.1

Kaplan, A., Kushnir, Y., Cane, M. A., & Blumenthal, M. B. (1997). Reduced space optimal analysis for historical data sets: 136 years of Atlantic sea surface temperatures. *Journal of Geophysical Research*, *102*(C13), 27835–27860. https://doi.org/10.1029/97JC01734

Kilbourne, K. H., Quinn, T. M., Webb, R., Guilderson, T., Nyberg, J., & Winter, a. (2008). Paleoclimate proxy perspective on Caribbean climate since the year 1751: Evidence of cooler temperatures and multidecadal variability. *Paleoceanography*, *23*(3). https://doi.org/10.1029/2008PA001598

Kuhnert, H., Crüger, T., & Pätzold, J. (2005). NAO signature in a Bermuda coral Sr/Ca record. *Geochemistry, Geophysics, Geosystems*, *6*(4). https://doi.org/10.1029/2004GC000786

Kuhnert, H., Patzold, J., Hatcher, B., Wyroll, K.-H., Eisenhauer, A., Collins, L. B., et al. (1999). A 200-year coral stable oxygen isotope record from a high-latitude reef off Western Australia. *Coral Reefs*, *18*, 1–12. https://doi.org/10.1007/s003380050147

Kuhnert, H., Pätzold, J., Wyrwoll, K.-H., & Wefer, G. (2000). Monitoring climate variability over the past 116 years in coral oxygen isotopes from Ningaloo Reef, Western Australia. *International Journal of Earth Sciences*, *88*(4), 725–732. https://doi.org/10.1007/s005310050300

Li, X., Liu, Y., Hsin, Y. C., Liu, W., Shi, Z., Chiang, H. W., & Shen, C. C. (2017). Coral record of variability in the upstream Kuroshio Current during 1953–2004. *Journal of Geophysical Research: Oceans*, *122*(8), 6936–6946. https://doi.org/10.1002/2017JC012944

Linsley, B. K., Dunbar, R. B., Wellington, G. M., & Mucciarone, D. A. (1994). A coral-based reconstruction of Intertropical Convergence Zone variability over Central America since 1707. *Journal of Geophysical Research*, *99*(C5), 9977–9994. https://doi.org/10.1029/94JC00360

Linsley, B. K., Messier, R. G., & Dunbar, R. B. (1999). Assessing between-colony oxygen isotope variability in the coral Porites lobata at Clipperton Atoll. *Coral Reefs*, *18*(1), 13–27. https://doi.org/10.1007/s003380050148

McGregor, H. V., & Gagan, M. K. (2004). Western Pacific coral $\delta^{18}O$ records of anomalous Holocene variability in the El Niño-Southern Oscillation. *Geophysical Research Letters*, *31*(11), 1–4. https://doi.org/10.1029/2004GL019972

Moses, C. S., Swart, P. K., & Rosenheim, B. E. (2006). Evidence of multidecadal salinity variability in the eastern tropical North Atlantic. *Paleoceanography*, *21*(3), 1–12. https://doi.org/10.1029/2005PA001257

Murty, S. A., Goodkin, N. F., Halide, H., Natawidjaja, D., Suwargadi, B., Suprihanto, I., et al. (2017). Climatic influences on southern Makassar Strait salinity over the past century. *Geophysical Research Letters*, *44*(23), 11967–11975. https://doi.org/10.1002/2017GL075504

Nakamura, N., Kayanne, H., Iijima, H., McClanahan, T. R., Behera, S. K., & Yamagata, T. (2009). Mode shift in the Indian Ocean climate under global warming stress. *Geophysical Research Letters*, *36*(23), 3–7. https://doi.org/10.1029/2009GL040590

Osborne, M. C., Dunbar, R. B., Mucciarone, D. A., Druffel, E., & Sanchez-Cabeza, J. A. (2014). A 215-yr coral $\delta^{18}O$ time series from Palau records dynamics of the West Pacific Warm Pool following the end of the Little Ice Age. *Coral Reefs*, *33*(3), 719–731. https://doi.org/10.1007/s00338-014-1146-1

Pfeiffer, M., Timm, O., Dullo, W. C., & Podlech, S. (2004). Oceanic forcing of interannual and multidecadal climate variability in the southwestern Indian Ocean: Evidence from a 160 year coral isotopic record (La Réunion, 55°E, 21°S). *Paleoceanography*, *19*(4), 1–14. https://doi.org/10.1029/2003PA000964

Quinn, T. M., Crowley, T. J., Taylor, F. W., Henin, C., Joannot, P., & Join, Y. (1998). A multicentury stable isotope record from a New Caledonia coral: Interannual and decadal sea surface temperature variability in the southwest Pacific since 1657 A.D. *Paleoceanography*, *13*(4), 412–426. https://doi.org/10.1029/98pa00401

Quinn, T. M., Taylor, F. W., & Crowley, T. J. (1993). A 173 year stable isotope record from a tropical south Pacific coral. *Quaternary Science Reviews*, *12*(6), 407–418. https://doi.org/10.1016/S0277-3791(05)80005-8

Quinn, T. M., Taylor, F. W., & Crowley, T. J. (2006). Coral-based climate variability in the Western Pacific Warm Pool since 1867. *Journal of Geophysical Research*, *111*(C11), 1–11. https://doi.org/10.1029/2005JC003243

Ramos, R. D., Goodkin, N. F., Siringan, F. P., & Hughen, K. A. (2017). *Diploastrea heliopora* Sr/Ca and $\delta^{18}O$ records from northeast Luzon, Philippines: An assessment of interspecies coral proxy calibrations and climate controls of sea surface temperature and salinity. *Paleoceanography*, *32*(4), 424–438. https://doi.org/10.1002/2017PA003098

Shen, G., Cole, J., Lea, D., Linn, L., Mcconnaughey, T., & Fairbanks, R. (1992). Surface ocean variability at Galapagos from 1936–1982: Calibration of geochemical tracers in corals. *Paleoceanography*, *7*(5), 563–588. https://doi.org/10.1029/92pa01825

Swart, K., White, S., Enfield, D., Dodge, E., & Milne, P. (1998). Stable oxygen isotopic composition of corals from the Gulf of Guinea as indicators of periods of extreme precipitation conditions in the sub-Sahara. *Journal of Geophysical Research*, *103*(C12), 27885–27891. https://doi.org/10.1029/98jc02404

Swart, P. K., Dodge, R. E., & Hudson, H. J. (1996). A 240-year stable oxygen and carbon isotopic record in a coral from south Florida: Implications for the prediction of precipitation in southern Florida. *PALAIOS*, *11*(4), 362–375. https://doi.org/10.2307/3515246

Swart, P. K., Healy, G. F., Dodge, R. E., Kramer, P., Hudson, J. H., Halley, R. B., & Robblee, M. B. (1996). The stable oxygen and carbon isotopic record from a coral growing in Florida Bay: A 160 year record of climatic and anthropogenic influence. *Palaeogeography, Palaeoclimatology, Palaeoecology*, *123*(1–4), 219–237. https://doi.org/10.1016/0031-0182(95)00078-X

Tudhope, A., Chilcott, C., McCulloch, M. T., Cook, E. R., Chappell, J., Ellam, R. M., et al. (2001). Variability in the El Niño-Southern Oscillation through a glacial-interglacial cycle. *Science*, *291*(5508), 1511–1517. https://doi.org/10.1126/science.1057969

Tudhope, A. W., Shimmield, G. B., Chilcott, C. P., Jebb, M., Fallick, A. E., & Dalgleish, A. N. (1995). Recent changes in climate in the far western equatorial Pacific and their relationship to the Southern Oscillation; oxygen isotope records from massive corals, Papua New Guinea. *Earth and Planetary Science Letters*, *136*(3–4), 575–590. https://doi.org/10.1016/0012-821X(95)00156-7

Urban, F. E., Cole, J. E., & Overpeck, J. T. (2000). Influence of mean climate change on climate variability from a 155-year tropical Pacific coral record. *Nature*, *407*(6807), 989–993. https://doi.org/10.1038/35039597

von Reumont, J., Hetzinger, S., Garbe-Schönberg, D., Manfrino, C., & Dullo, C. (2018). Tracking interannual- to multidecadal-scale climate variability in the Atlantic Warm Pool using central Caribbean coral data. *Paleoceanography and Paleoclimatology*, *33*(4), 395–411. https://doi.org/10.1002/2018PA003321

Wellington, G. M., Schrag, D. P., Ren, L., Salinger, M. J., Tudhope, A. W., & Linsley, B. K. (2004). Geochemical evidence from corals for changes in the amplitude and spatial pattern of South Pacific interdecadal climate variability over the last 300 years. *Climate Dynamics*, *22*(1), 1–11. https://doi.org/10.1007/s00382-003-0364-y

Zinke, J., Dullo, W. C., Heiss, G. A., & Eisenhauer, A. (2004). ENSO and Indian Ocean subtropical dipole variability is recorded in a coral record off southwest Madagascar for the period 1659 to 1995. *Earth and Planetary Science Letters*, *228*(1–2), 177–194. https://doi.org/10.1016/j.epsl.2004.09.028

Zinke, J., Loveday, B. R., Reason, C. J., Dullo, W. C., & Kroon, D. (2014). Madagascar corals track sea surface temperature variability in the Agulhas Current core region over the past 334 years. *Scientific Reports*, *4*(1), 1–8. https://doi.org/10.1038/srep04393

Zinke, J., Rountrey, A., Feng, M., Xie, S. P., Dissard, D., Rankenburg, K., et al. (2014). Corals record long-term Leeuwin current variability including Ningaloo Niño/Niña since 1795. *Nature Communications*, *5*, 1–9. https://doi.org/10.1038/ncomms4607